NASA Technical Memorandum 4231

Analytical and Photogrammetric Characterization of a Planar Tetrahedral Truss

Chauncey Wu, Richard R. Adams,
and Marvin D. Rhodes

DECEMBER 1990

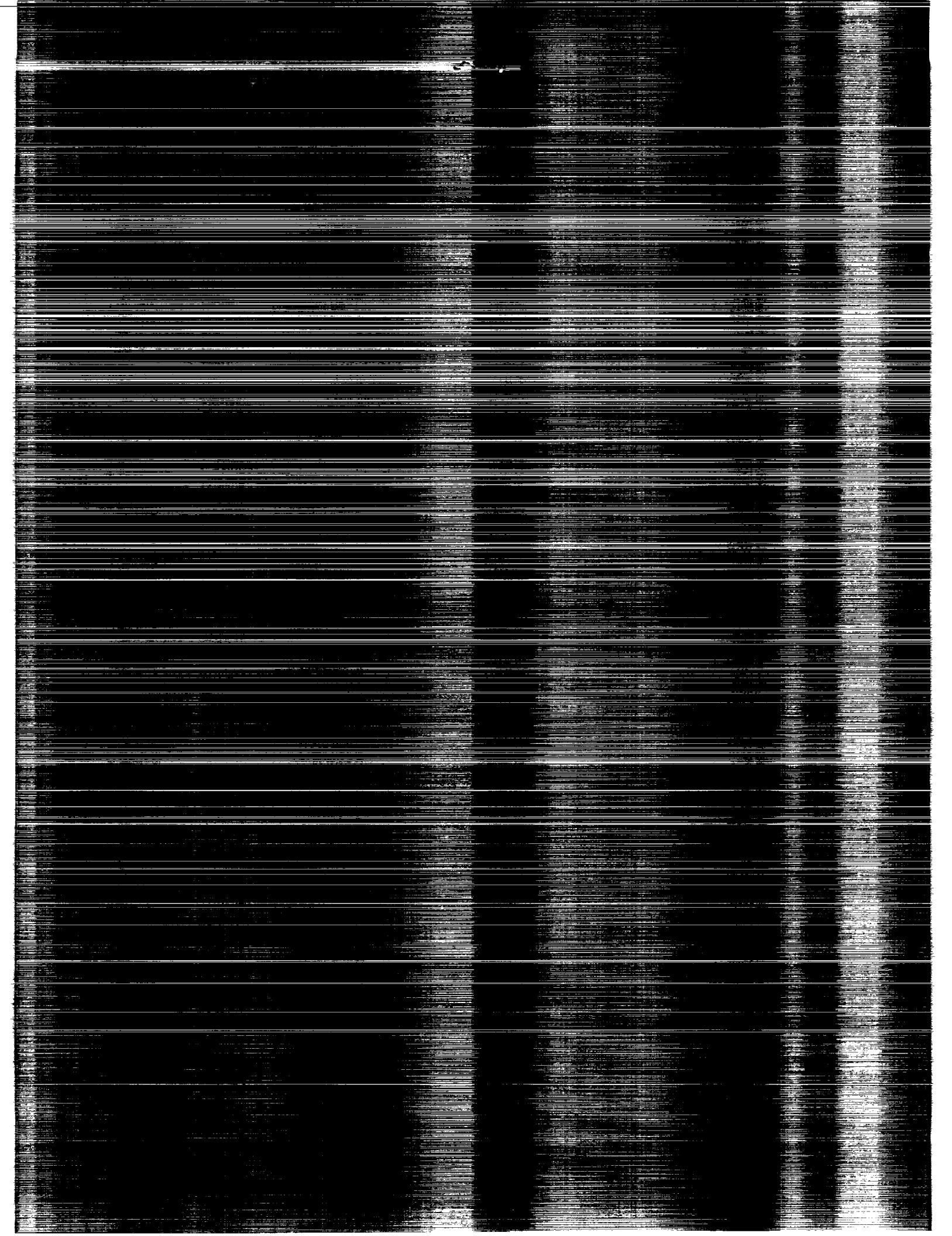

NASA Technical Memorandum 4231

Analytical and Photogrammetric Characterization of a Planar Tetrahedral Truss

K. Chauncey Wu, Richard R. Adams,
and Marvin D. Rhodes
Langley Research Center
Hampton, Virginia

National Aeronautics and
Space Administration
Office of Management
Scientific and Technical
Information Division

1990

Summary

Future space science missions are likely to require near-optical quality reflectors which are supported by a stiff truss structure. This support truss should conform closely with its intended shape to minimize its contribution to the overall surface error of the reflector. The current investigation was conducted to evaluate the planar surface accuracy of a regular tetrahedral truss structure by comparing the results of predicted and measured node locations. The truss is a two-ring hexagonal structure composed of 102 equal-length truss members. Each truss member is nominally 2 m in length between node centers and is comprised of a graphite-epoxy tube with aluminum nodes and joints. The axial stiffness and the length variation of the truss components were determined experimentally and incorporated into a static finite element analysis of the truss. From this analysis, the root-mean-square (rms) surface error of the truss was predicted to be 0.11 mm. Photogrammetry tests were performed on the assembled truss to measure the normal displacements of the upper surface nodes and to determine if the truss would maintain its intended shape when subjected to repeated assembly. Considering the variation in the truss component lengths, the measured rms error of 0.14 mm in the assembled truss is relatively small. The test results also indicate that a repeatable truss surface is achievable. Several potential sources of error were identified and discussed.

Introduction

Future deep-space and Earth science missions are likely to require large diameter, stiff trusses to provide an accurate support structure for attachment of an optical or near-optical quality reflector surface (refs. 1 and 2). The large size of these structures will preclude their transportation to orbit in an operational configuration; therefore, they must be deployed or constructed in Earth orbit. The support structure should have a high stiffness to minimize low-frequency structural vibrations (induced by station keeping or tracking and pointing loads) which could make control of the spacecraft difficult. The support truss must also conform closely to its intended shape to minimize its contribution to the overall error of the reflector. Because the support truss surface errors are likely to have a large effect on the accuracy of the reflective surface, it is desirable to be able to analytically predict and experimentally verify the attachment point locations of this class of structure prior to use in space-flight applications.

In this study, the upper surface quality of a planar tetrahedral truss is evaluated by comparing predicted nodal displacements with measured values determined from photogrammetry. The geometry of this truss is similar to structures proposed for use in the spacecraft described previously. The truss hardware studied is the focus of an experiment designed to evaluate the potential for automated assembly of large space structures (ref. 3). For the purposes of the current study, the surface error is considered to be the normal displacement of the center of the nodes from an ideal plane. The displacement of each node was predicted with a finite element analysis and measured experimentally with convergent close-range photogrammetry. The nodal displacements predicted are compared with the experimental values observed. The axial stiffness of the truss members was experimentally determined and incorporated into the finite element model. Variations in the length of individual truss components which resulted from the manufacturing and fabrication processes were measured and also incorporated in the analysis. Modeling of these member errors is described and the effect of variations in length on the predicted accuracy of the truss surface is examined. Potential error sources are also presented and discussed.

Truss Description

A planform view of a model of the planar truss structure evaluated in this study is shown in figure 1. The truss is defined as a two-ring structure, where the two concentric hexagonal rings (labeled as the inner and outer rings) on the truss upper surface are shown in sketches in the figure. The truss is comprised of 102 members of the same nominal length connected at 31 nodes. Each node is designed to accommodate up to nine truss members: six members in the surface plane of the truss and three members in the core that connect the planes together. The load axes of all nine truss members intersect at the geometric center of the node.

The assembled truss structure is shown in figure 2 mounted on a rotating turntable in the automated assembly facility. Each truss member is 2 m between node centerlines and is comprised of a 1.74-m-long graphite-epoxy tube (with an outer diameter of 2.64 cm and an inner diameter of 2.22 cm), two joint assemblies (each 9.9 cm in length), and two nodes with preattached receptacles. The material used in the graphite tube is T300/934[1] with a $[\pm 10°]_8$ layup. With a composite laminate analysis, the predicted axial elastic modulus of the tube material is 126.3 GPa which, when multiplied by the

[1] T300 graphite is manufactured by Union Carbide Corporation; aerospace adhesive EA 934 is manufactured by Hysol Division, Dexter Corporation.

cross-sectional area of 1.60 cm^2, is equal to a tube cross-sectional stiffness $(EA)_t$ of 20.2 MN.

Two aluminum joints, similar to those shown in figure 3, were bonded to each end of a graphite-epoxy tube with an epoxy resin. This unit is hereafter referred to as a strut. To assemble the strut in the truss, the mushroom-shaped connector on the joint is inserted into a receptacle which is preattached to the node with a threaded stud. This unit is referred to as a node for the axial stiffness tests. The joint is simultaneously preloaded and locked by turning a locking nut which protrudes from the side of the joint. Approximately 2.26 N-m of torque is required to lock and preload the joint to a nominal value of 0.89 kN. The internal mechanism of the joint is shown in figure 4. Turning the locking nut draws the connector into the joint body and compresses a set of Belleville spring washers inside the joint. This action also advances the ramped surface ahead of the wedge until it bears against the receptacle. The mechanical system eliminates any free play in the joint and provides a compressive preload across the receptacle-joint connection.

Strut Experimental Evaluation

Test Description

To accurately model the truss structure with finite element techniques, it was necessary to experimentally determine the axial stiffness of a representative sample of the struts. Seven struts were selected at random for testing from the 113 units fabricated. The struts were assembled for testing by locking the joints into two nodes as described earlier. The same two nodes were used throughout the test program. A schematic and photograph of the axial test setup are shown in figure 5. The assembled test specimen was placed between two vertical brackets which were attached to a stiff steel backstop. A load cell was placed between the upper end of the test specimen and a fixed upper bracket as shown in figure 6(a). The lower end of the test specimen was attached to a displacement-control manual jackscrew loading system, the base of which was also affixed to the backstop as shown in figure 6(b).

The load-displacement response of the two joints and the graphite-epoxy tube was monitored separately during the test. Three direct-current displacement transducers (DCDT's) were placed at 120° intervals around each joint section as shown in figures 6(a) and (b). The effective joint length over which the displacements were measured was 12.7 cm and included the entire joint mechanism, the joint-receptacle interface, and the threaded connection between the receptacle and node. The stiffnesses of the node and receptacle were significantly higher than that of the joint mechanism. Consequently, most of the deflection in the system was assumed to occur in the joint mechanism. The DCDT core probes for the tube were suspended from the mounting plate on the upper joint section with monofilament line. Small lead weights were attached to keep the line in tension. The effective tube length was measured between the DCDT mounting plates on the upper and lower joint sections and included the epoxy bonds between the tube and joints.

The manual loading system used in these tests consisted of a geared mobile platform which translated vertically on a bracket fixed to the backstop. By rotating a handle, the lower node was incrementally displaced, resulting in an incremental load in the test specimen. The axial load in the member was usually increased to +1.11 N tension, unloaded through zero to −1.11 kN compression and then loaded back to the zero-load position. Several tests were conducted with the order of loading reversed (i.e., from compression to tension). Experimental data are given in terms of an effective cross-sectional stiffness (EA), the product of the elastic modulus E and cross-sectional area A. This notation is used because the cross section of the joint varies along its length.

Load and displacement data from the load cell and DCDT's were collected and processed with a personal-computer-based data collection system. In addition, the load cell readout was displayed on a voltmeter to provide real-time information on the load in the truss member. The data manipulation was performed with a spreadsheet program on a personal computer.

Strut Test Results

Tube axial stiffness. An experimental load-displacement curve representative of the seven graphite-epoxy strut tubes tested is shown in figure 7. The displacement shown in the figure is the average of the axial displacement measured by the three DCDT gauges to negate the effect of any bending that may occur in the section. The irregularity in the test data is probably due to friction between the probe and barrel in the DCDT's, stiction in the loading mechanism, and the associated dynamic response characteristics of the instrumentation, as well as manual control of the displacement mechanism. A slight bilinearity in the tube stiffness (typical of composite materials) was observed in the test data, with a slightly lower stiffness in tension than in compression. A line which best represents the average slope of the test curve is also shown drawn in the figure. The slope of this line is taken as the axial stiffness

of the strut tube. The average axial stiffness of the seven graphite-epoxy tubes tested was 10.0 MN/m with a variation of −1.9 to +3.2 percent. This corresponds to a cross-sectional tube stiffness $(EA)_t$ of 17.4 MN, which is 13.9 percent less than the stiffness predicted by laminate analysis. This decrease is probably the result of a higher matrix volume fraction in the actual tube than the properties assumed for the laminate analysis.

Joint stiffness. Axial stiffness results were obtained from the 14 mechanical joints on the seven test struts. Examples of the experimental results obtained are shown in figure 8. In contrast to the results obtained for the graphite tubes, considerable variation was obtained in the response of the 14 test joints. As noted previously, the average displacement from the three DCDT readings was taken for each joint section and plotted against the axial load to generate the load-displacement plot. The joint represented in figure 8(a) has a load-displacement response that is anticipated based on the design aspects of the joint. The local irregularities in the response curve are similar to those observed in the tube response curve and are probably due to the same factors noted. The stiffness is nominally linear as the joint is loaded in tension until the preload level is reached at about 890 N. At this applied load the stiffness is dramatically reduced. The response in compression is similar to the initial tensile response and the stiffness is constant for the test range. The straight line shown in figure 8(a) has been drawn through the data from −1.33 to +0.89 kN and is taken to be representative of the joint cross-sectional stiffness $(EA)_j$ of 5.38 MN.

The results shown in figure 8(b) are significantly different from those in figure 8(a). The two data sets are a sample of the test results obtained. The joint shown in figure 8(b) had a lower preload, as evidenced by a much lower slope of the tensile response compared with the compression response, even though the nut closure torque was the same for all test components. The compression response, however, was similar to that of the joint in figure 8(a). The reduced tensile stiffness and the substantial hysteresis observed in figure 8(b) are the result of low initial loads in the Belleville washers which were set during fabrication of the joint (fig. 4) and determined the tensile preload limit and stiffness. When the joints were fabricated, the procedure for setting the load in the Belleville washers permitted substantial variation in the tensile preload which was realized only as a result of these tests. Unfortunately, this could not be changed or modified after the joint was bonded to the graphite tube. The compressive stiffness values measured during the joint tests were more consistent and repeatable than the corresponding measured tensile values. Since all the joints had the same nominal compressive stiffness and only some had the same stiffness in tension, the measured compressive joint cross-sectional stiffness of 5.38 MN was assumed to represent all the joints in the finite element model.

Effective strut stiffness. An estimate of the effective cross-sectional stiffness of a complete truss member was computed by considering the truss member to be three axial springs connected in series. With a series-spring representation, the effective axial stiffness of the truss member $(EA)_e$ is

$$(EA)_e = \frac{L(EA)_j(EA)_t}{2(EA)_t l_j + (EA)_j l_t} \tag{1}$$

where $(EA)_j$ is the axial stiffness of the two mechanical joints and $(EA)_t$ represents the axial stiffness of the graphite-epoxy tube. The terms l_j, l_t, and L are the node centerline-to-joint bondline length, the graphite-epoxy tube length, and the overall truss member length, respectively. With the use of experimentally determined axial stiffnesses for the truss member components, the effective axial stiffness of the truss member is 13.6 MN, or approximately 75 percent of the stiffness of the graphite-epoxy tube; this indicates that the joint axial stiffness has a significant effect on the overall stiffness of the truss member. The influence of the joints is due to the relatively long joint length (13 percent of the 2-m member length) and the relatively low stiffness of the joint (30 percent of the graphite-epoxy tube stiffness).

Truss Component Measurements

The truss components were measured to determine dimensional variation in their length and its effect on node location by using numerically controlled validation machines and other precision measurement instruments. Each truss component (i.e., the nodes, struts, and joint receptacles) was given a unique identification number and the size of the component was measured and recorded. The average length of each component type was determined and the difference between the measured value and the average value was taken as the manufacturing length error. This technique for determining component error is suitable for evaluating the planar accuracy of this truss because each truss member has the same nominal length. Consequently, a change in the average length of the truss members will only cause a uniform expansion or shrinkage of the structure but will not induce asymmetric geometric distortions in the truss. The results of this aspect of the investigation are discussed briefly here.

Nodes

The nodes (fig. 3) were measured across each of the three hexagonal face diameters in the plane surface. The three across flat diameters on each node were measured with an electromechanical micrometer which has a resolution capability of ± 2.5 μm. The three values for any given node were generally within ± 5.0 μm. However, the variation from node to node was generally in the range of ± 76.0 μm. Due to the relative high machining precision measured on each node, it was assumed that the distance from the geometric center of the node to each of the nine receptacle attachment facets was one half the average distance measured across the six coplanar facets of the node.

For experimental measurement of the truss node positions, close-range photogrammetry was employed, requiring fabrication and mounting of position targets. A set of steel bolts was machined for mounting targets on the nodes of the truss upper surface. One such mount with the target attached is shown in figure 9. The node faces have threaded holes and cruciform slots which were used as positioning guides during fabrication of the nodes. A steel bolt was threaded directly into this hole after the retroreflective target was placed in the center of the bolt head. The height of the target from the node center was determined for each of the 19 upper surface nodes with a numerically controlled measuring machine, which has a measurement precision of ± 2.5 μm.

Joint Receptacles

The joint receptacles (fig. 3) were measured to determine the variation in length with the same micrometer as was used to measure the node diameters. The length measurement was taken from the face which bears on the node facet to a point on the plane in compressive contact with the assembled joint.

Strut

The struts were measured with a large-field (1.2 by 1.8 m) numerically controlled machine which has a measurement precision of ± 8.0 μm. Since the contact surfaces in the joint move when the locking torque is applied, two receptacles (without the nodes attached) were attached to the strut and the joints were locked to them. The strut length was taken to be the perpendicular distance between the centers of the receptacle faces minus the length of the receptacles.

Effective Member Length

The length variation in the assembled truss members was determined from the sum of the measured length variations of the components. The aggregate length error ε in each member is given by

$$\varepsilon_{\text{tot}} = \frac{1}{2}(\varepsilon_{n1} + \varepsilon_{n2}) + \varepsilon_{r1} + \varepsilon_{r2} + \varepsilon_{\text{strut}} \qquad (2)$$

where the subscripts n and r indicate the nodes and receptacles, respectively. The contribution of one half the error at each node to the total error follows from the assumption that the variation in the node diameter is equally distributed around the node's geometric center.

Finite Element Analysis

A linear finite element analysis was performed on a model of the truss to analytically predict the deformed shape of the truss upper surface. For many proposed space applications, the normal displacement of the truss nodes from the design contour is of current interest because it gives an indication of the magnitude of the adjustments which may have to be made to achieve a minimum total surface error. Since a rigid-body displacement and/or rotation of the entire truss may be performed to align the truss, the surface error normal to the best-fit plane through all the upper surface nodes is considered to be the surface error in this paper. Deviation from a planar surface is caused by a combination of internal member loads (caused by length variations between the individual truss members) and a uniform gravity loading of the truss.

Model Description

The finite element model of the truss was developed and analyzed with Engineering Analysis Language (EAL). A discussion of EAL can be found in reference 4. A sketch illustrating important aspects of the model is shown in figure 10. Axial stiffness elements were used to represent the truss members. The effective truss member axial stiffness $(EA)_e$ (determined from component tests) of 13.6 MN was used as input to the analysis model. The node and joint masses were modeled as point masses located at the node locations, whereas the strut mass was distributed equally to the two connected nodes. Pinned boundary conditions (all three translational degrees of freedom restrained) were applied at the three central nodes in the lower plane of the truss. These boundary conditions are intended to represent the bolted attachments which connect the truss to the turntable support fixture.

As indicated previously, the individual truss components were all numbered and their individual location in the truss structure was cataloged during assembly. The measured length errors in the

truss components were modeled as thermally induced strains in the finite element model. The applied thermal load ΔT for each truss member is

$$\Delta T = \frac{\varepsilon_{tot}}{\alpha L} \tag{3}$$

where α is an arbitrary material coefficient of thermal expansion, L is the nominal member length (between node centerlines), and ε_{tot} is the total length variation for that member (as defined by eq. (2)).

Predicted Node Positions and Member Loads

A static finite element analysis was conducted on the truss under a combination of gravity loading and member length errors. The numbering sequence for the 19 upper surface (X-Y plane) nodes is shown in figure 11. The analytically predicted normal displacement for the upper surface nodes is shown as a function of node number in figure 12(a) and in an axonometric projection in figure 12(b). Each predicted displacement is referenced to the average Z-displacement. This is equivalent to referencing the data to a "best-fit plane" having zero in-plane rotations and an out-of-plane translation equal to the average Z-displacement. This assumption is justified by noting that a six-parameter (three rotations and three translations) best-fit plane through the upper surface indicates that the in-plane rotations are on the order of 10^{-7} radians and, therefore, negligible. Considering that the analysis includes the effect of gravity and that traditional dimensional accuracy requirements were used in the manufacturing of the truss components, the predicted displacements seem to be small. Of the 19 nodes, all but 5 are within about 0.13 mm (0.005 in.) of the best-fit plane, and from the projection in figure 12(b), these errors do not appear to have a bias. Any significant in-plane rotation of the truss would appear as a bias in the axonometric projection. The root mean square (rms) of the differences of the upper surface nodes is 0.11 mm. The predicted nodal displacements for the truss with and without member length errors are shown in table 1(a). The rms error of 0.02 mm for the truss with equal length members is due strictly to the gravity load, whereas the surface error in the truss with member length errors is dominated by the imperfections in the truss members. The maximum predicted tensile load in the truss is 0.44 kN and occurs in an upper surface member, whereas the largest compressive load is 0.33 kN and occurs in a core strut. Ten struts have predicted internal loads higher than 0.22 kN in tension.

Parametric Analysis

The effect of varying the member stiffness on the truss upper surface displacements was also studied with the analytical model described previously. Since there was a significant variation in the joint tensile stiffnesses (as well as a much smaller variation in the stiffness of the graphite-epoxy tubes) observed during the component tests, changing the effective stiffness of the truss member in the finite element model should give an indication of the sensitivity of the truss surface to any variation in the component stiffnesses. Reductions in the effective axial stiffness of all truss members of 10 and 20 percent from the nominal value of 13.6 MN were applied. These correspond to reductions in the axial stiffness of the joint population of 26 and 45 percent, respectively. The largest difference in the predicted normal displacement of the nodes (for a 20-percent axial stiffness reduction) was 0.02 mm at 2 of the 19 upper surface nodes; this indicates little sensitivity to variation in the truss member axial stiffness. This observation suggests that, for the truss member stiffness reductions studied, any out-of-plane deviation of the upper surface nodes is driven by the variation in the truss member lengths rather than the stiffness of the truss members. However, another factor which was not evaluated in this investigation and may be of importance is the effect of variation in stiffness from member to member on the upper surface planarity.

Experimental Node Position Measurement

Three sets of measurements were taken of the assembled truss structure to locate the spatial coordinates of the high-contrast retroreflective targets on each of the 19 upper surface nodes with convergent close-range photogrammetry. The data were obtained from full coverage metric camera photographs of the target field taken from 24 different vantage points above the truss. The truss was disassembled and reassembled between the second and third measurement sets to determine the repeatability achievable with the existing hardware.

The photogrammetry system used for the planning, execution, and analysis of the data is a commercially available system known as the Simultaneous Triangulation and Resection System (STARS), developed by Geodetic Services, Inc. (GSI). A brief overview of the photogrammetric principles involved in these measurements is presented; a rigorous discussion of the theory, equations, hardware, and software of STARS may be found in reference 5, with a more general discussion in reference 6.

Test Methodology

Photogrammetry is based on a simple pair of equations, herein called the projective equations. These equations relate the two-dimensional measured coordinates (x, y) of target images and the corresponding object space coordinates (X, Y, Z) of the targets photographed in terms of several constants, often referred to as the projective parameters. The projective equations are derived from geometrical optics on the basis of two fundamental assumptions, namely

1. All target images lie in a common image plane
2. The photographed target in object space, its image, and the center of projection of the lens all lie on a straight line

For the case of a multistation, single camera network, the projective parameters for each station include the (X, Y, Z) coordinates of the center of projection in object space and the three rotation angles defining the orientation of the axes of image space with respect to those of object space. The projective parameters for the camera include the three coordinates of the center of projection in image space. Lens distortions, although considered as systematic errors, have been shown to be dependent upon the target distances from the camera and, as such, are best modeled as parameters to be solved for in the projective equations. Thus five lens distortion coefficients (three radial and two decentering) are considered in the STARS adjustment as additional parameters for camera self-calibration.

A pair of projective equations is generated for each target image on each photograph. Thus, if the image coordinates (x, y) for each of n targets are observed on each of m photographs, a system of $2mn$ projective equations will result. Besides the $3n$ unknowns (X, Y, Z) for the object space coordinates of the targets, the projective equations carry the $6m$ station parameters, the 3 camera parameters and the 5 additional parameters to account for lens distortion as unknowns.

Computer simulations were used to plan the photogrammetric network required to achieve the desired measurement precision. Traditional photogrammetric practice suggests that the ratio of measurement precision to hardware tolerance be at least 1:5, and preferably 1:10, to accommodate statistical fluctuations in the measurement results. Therefore, a network measurement precision goal of 0.03 mm was established. This corresponds to a proportional accuracy of one part in 315 000 of the truss diameter. With a conservative value of 2.0 μm as the overall image measurement precision and the design coordinates for the target node locations, it was found that the measurement goal should be attainable by using 12 camera stations at each of 2 elevations above the top of the truss. Sufficient data to assure lens self-calibration were obtained by incrementing the lens roll angle by 30° between each station. Optimum lens focus distance and optimum target diameter, as well as predicted precisions for the recovery of camera and station parameters and the corresponding effect of the propagation of these uncertainties into the recovered target coordinates, resulted in the complete plan for the test.

Test Description

Metric photography was accomplished with a large format metric camera fitted with a 240-mm lens cone focused to a distance of 11.0 m at an aperture of $f/32$. The camera was mounted on a heavy-duty pan-tilt tripod which was secured to the platform railing of a high-lift platform. The truss was rotated about the Z-axis in 30° increments between each metric photograph by using the supporting base turntable. The 12 photographic stations were taken at elevations of 7.0 and 8.8 m above the top of the truss at a horizontal distance of 7.9 m from the truss center of rotation. Illumination was provided by a 200-W-sec strobe lamp mounted to the camera.

Target mounts for the nodes shown in figure 9 and discussed previously were located at the center of the top 19 nodes of the truss. Disks of retroreflective tape were affixed to the top of each mount and covered by opaque donut pad masks, which were carefully centered (by eye inspection) over the mounts. Additional secondary targets were placed below the assembly on the top of the rotating table to provide geometric depth for strengthening the recovery of projective parameters during the data analysis. The target node location numbers are the same as those used in the finite element analysis shown in figure 11.

Data Reduction and Analysis

The (x, y) coordinates of each target on each of the data photographs were measured to a precision of 0.5 μm with a STARS Autoset monocomparator. This was accomplished in two stages. First the target coordinates from four stations separated by 90° and photographed from the higher elevation were read in a semi-automatic mode. These data were then merged with the design coordinates of the top nodes as control, and a preliminary resection was completed, recovering improved estimates of the station parameters for each of the four selected stations. The initial object space coordinates for each target were then generated by a preliminary triangulation.

The second stage was conducted with the automatic resection driveback feature of the automatic precision monocomparator, and a complete observation of the remaining data frames was obtained for all measurements. The image coordinates for each data frame were preprocessed to correct for systematic errors introduced by film distortion and the calibration function of the comparator.

The objective of the photogrammetry measurements was to provide a basis for evaluation of the quality of the plane across the top of the truss and to assess the positioning repeatability of the truss. For these measurements, a free network iterative least-squares bundle adjustment (ref. 7) with self-calibration was performed on the data with the STARS photogrammetric software. In the free network adjustment, the object space coordinate system is not explicitly defined but rather is iteratively established so as to generate a covariance matrix of the entire set of triangulated coordinates having a minimum trace (sum of diagonal elements). In this sense, the coordinate system is defined implicitly to produce results of highest overall precision. Accordingly, all points participate equally in the definition of an object space coordinate system, preserving the mean position, mean orientation, and mean scale of the network with respect to the approximate starting values of the targets. This adds seven additional parameters (defining a unique implicitly scaled object space coordinate system) to the number of unknowns carried in the projective equations.

The initial data set to evaluate the quality of the plane across the top surface of the truss consisted of a system of $2mn$ projective equations to solve for $(3n+6m+3)$ projective parameters and 12 additional parameters. Since there were 24 stations ($m = 24$) used to measure 34 targets ($n = 34$), a total of 1632 equations were generated having only 261 unknowns. The bundle adjustment software exploits this over-determination by employing the method of least squares to extract from the set of projective equations a reduced set of equations (the normal equations) leading to results of greatest precision. Although the unknown parameters are determined from the solution of the normal equations, the square roots of the diagonal elements of the inverse of the coefficient matrix of the normal equations provide the corresponding standard errors.

The second data set to evaluate assembly repeatability involved two measurements which were conducted and reduced identically, including a preliminary 24-station bundle adjustment for each case. A final free network adjustment was executed wherein the two data sets were combined. The principal advantage of using a single reduction, when comparing two epochs photographed with the same metric camera, is strengthened self-calibration of the camera. The top 19 node targets for the second set were temporarily relabeled to ensure independent recovery of their coordinates during the simultaneous reduction, whereas the targets located on the table were common to both measurements. Since the maximum number of stations accommodated by the software is 40, the 20 strongest stations, as indicated by the station residuals from the preliminary adjustments, were selected for the final combined reduction. In this case the final reduction involved the solution of 2720 equations for 414 unknowns.

Free network adjustment results, while approximately preserving the preferred coordinate system sense and scale, are obtained in an arbitrary coordinate system. The STARS Rigid Body transformation module, a rigorous similarity coordinate transformation, was used to best overlay, in a least-squares sense, the photogrammetric results for each measurement with the design coordinates of the top 19 nodes of the truss.

Test Results and Correlation

The results from the initial photogrammetry measurement are listed in table 1(b) and the normal (Z) displacements are shown in figure 13. The nodal displacements are plotted as a function of node number in figure 13(a) and are shown in an axonometric projection in figure 13(b). Also, the predicted node displacements from the finite element analysis are shown in the figures for comparison. The photogrammetry measurement precision of 0.03 mm rms is shown superimposed on the results in figure 13(a). There is a difference of 0.03 mm between the rms displacements of measured and predicted node positions, as shown in table 1(b). A comparison of the predicted and measured displacements at each node indicates that approximately 25 percent of the measured values agrees with the predicted values to within the precision of the measurement technique. The largest differences between measured and predicted values are 0.18 mm and 0.13 mm which occur at nodes 8 and 4, respectively. Note that the rms values for the differences listed in table 1(b) are the root mean square of the differences between the measured and predicted results, and not the difference of the individual root mean squares. The axonometric projection in figure 13(b) indicates that there is no apparent bias in the results and that there are similar trends in the predicted and measured results.

There are several potential sources of variation in component size that may contribute to errors in the analytical prediction of the node locations. One source is the experimental strut member length data.

Any discrepancies in these data would lead directly to errors in the finite element analyses and a corresponding lack of correlation with the experimental displacements. Errors in strut length could result from two conditions: One is curvature in the truss members, and a second is axial misalignment of the aluminum joints when they were bonded to the graphite tubes. Either of these conditions directly results in errors in determining the variation in length of strut members. A second source of variation in component size could be environmental contamination on the mating surfaces of the truss components. After the components were measured to determine the size variation, they were stored in a test laboratory and no special provisions were made to keep the contact surfaces free from particulate contamination. A third error source is associated with the surface texture of the individual components. When the components were measured, a small probe was used to contact the surface at approximately the same location on each unit. In the assembled condition, larger surface areas are in contact. Therefore, any variations in texture and general waviness in nominally flat surfaces can contribute to differences in component and assembled member lengths.

Other sources which could contribute to variations between predicted and measured node displacements are the boundary conditions imposed on the finite element model and variation in the preload of the truss joints. It was assumed in the analysis model that the base support nodes were pinned; however, the experimental test condition is probably better represented as a flexure member, the stiffness of which was not experimentally determined. As for the joint preload, analysis studies were performed to evaluate the effect of uniform changes in stiffness at every joint; however, no studies were conducted where individual joints had major differences in stiffness similar to those observed during tests of the 14 experimental joints. None of these error sources is easy to quantify and relate directly to the observed differences between predicted and measured node positions.

Two sets of photogrammetry tests were performed to determine if assembly and disassembly of the truss would affect the upper surface node locations. For this test the truss was assembled and the joints were locked in a regular, repeatable order. Following the photogrammetry measurement, the joints were all unlocked and then relocked in exactly the same order and to the same torque value as the prior assembly, and a second measurement was obtained. The results of the measurements are presented in figure 14, which has a similar format to photogrammetry results presented previously. The photogrammetry results listed in table 2 indicate that the position of the top surface nodes is generally repeatable. The difference between the rms value of the two measurements is 0.02 mm. In addition, note that the individual displacements for all but two nodes (nodes 4 and 12) are well within the 0.03-mm measurement precision of the photogrammetry test.

The displacements from the repeatability tests were also averaged and compared with the displacements that were predicted by finite element analysis. The results are shown in figure 15. The analytical rms displacement increased slightly from its initial value because several of the struts were different from those in the initial model. The correlation between the average measured photogrammetry data and the analytically predicted results is similar to those discussed previously.

It was previously noted that, for precision space reflectors, the support truss must conform closely to its intended shape to minimize its contribution to the overall reflector error. When considering the level of accuracy imposed during component manufacturing, the rms error between the assembled truss and a best-fit plane appears to be moderate. However, from the comparison of measured and predicted individual node positions in figures 13 and 14, it is apparent that additional work in this area is required. The error sources noted are (1) strut length error due to curvature and joint misalignment, (2) contamination of mating surfaces, (3) surface texture variations, (4) modeling of boundary conditions, and (5) variation in individual joint stiffness, as well as other sources which may not have been identified. These issues should be explored further and their effects quantified.

Concluding Remarks

Future space science missions are likely to require near-optical quality reflectors which are supported by a stiff truss structure. This support truss should have a shape which conforms closely with its intended shape to minimize its contribution to the overall surface error of the reflector. The current investigation was conducted to evaluate the planar surface accuracy of a regular tetrahedral truss structure by comparing the results of predicted and measured node locations. The truss is a two-ring hexagonal structure composed of 102 truss members. Each truss member is comprised of a graphite-epoxy tube and aluminum node and joint hardware. Each truss member is nominally 2 m in length between node centers. The axial stiffness of the truss components was experimentally determined from a random sample of the truss members. The effective truss member axial stiffness

was found to be approximately 75 percent of the axial stiffness of the graphite-epoxy tube. The length variation in the assembled truss members was determined from precision measurements of the structural components. Both the member axial stiffness and length variation data were incorporated into a static finite element analysis of the truss. From this analysis, the root-mean-square (rms) surface error of the truss was predicted to be 0.11 mm.

Photogrammetry tests were performed on the assembled truss to measure the normal displacements of the upper surface nodes and to determine if the truss would maintain its intended shape when subjected to repeated assembly. Considering the variation in the truss component lengths, the measured rms error of 0.14 mm in the assembled truss is relatively small. The test results also indicate that a repeatable truss surface is achievable. However, the comparison of the predicted and measured displacements indicates a rms difference of approximately 0.03 mm. Several potential sources of error were identified which may account for this difference. These sources should be further explored and their effects quantified.

NASA Langley Research Center
Hampton, VA 23665-5225
November 1, 1990

References

1. *The Large Deployable Reflector (LDR) Report of the Science Coordination Group.* JPL Publ. 86-46, California Inst. of Technology, 1986. (Available as NASA CR-180235.)
2. Rowell, Lawrence F.; and Swissler, Thomas J.: *Advanced Technology Needs for a Global Change Science Program—Perspective of the Langley Research Center.* NASA TM-4196, 1990.
3. Rhodes, Marvin D.; Will, Ralph W.; and Wise, Marion A.: *A Telerobotic System for Automated Assembly of Large Space Structures.* NASA TM-101518, 1989.
4. Whetstone, W. D.: *EISI-EAL Engineering Analysis Language Reference Manual—EISI-EAL System Level 2091. Volume 2: Structural Analysis—Primary Processors.* Engineering Information Systems, Inc., July 1983.
5. Brown, Duane C.: *Application of Close-Range Photogrammetry to Measurements of Structures in Orbit,* Volume 1. GSI Tech. Rep. No. 80-012 (Contract No. MOM7DNS-895942), Geodetic Services Inc., Sept. 15, 1980.
6. Slama, Chester C., ed.: *Manual of Photogrammetry,* Fourth ed., American Soc. of Photogrammetry, c.1980.
7. Papo, H. B.; and Perelmuter, A.: Free Net Analysis in Close-Range Photogrammetry. *Photogramm. Eng. & Remote Sens.,* vol. 48, no. 4, Apr. 1982, pp. 571–576.

Table 1. Predicted and Measured Node Positions

(a) Predicted from finite element analysis with gravity load

Node	Equal length members			Measured errors in members		
	X, mm	Y, mm	Z, mm	X, mm	Y, mm	Z, mm
1	0.00	0.00	0.05	−0.01	0.05	0.18
2	1000.00	1732.05	0.01	1000.02	1732.09	0.08
3	−1000.00	1732.05	0.01	−999.97	1732.15	−0.07
4	−2000.00	0.00	0.01	−1999.98	0.12	−0.01
5	−1000.00	−1732.06	0.01	−1000.03	−1732.05	0.17
6	1000.00	−1732.06	0.01	1000.04	−1732.02	0.08
7	2000.00	0.00	0.01	2000.01	0.07	0.01
8	2000.00	3464.11	−0.02	1999.95	3464.21	0.03
9	0.00	3464.11	−0.01	0.02	3464.08	−0.13
10	−2000.00	3464.11	−0.02	−1999.91	3464.24	−0.25
11	−3000.00	1732.05	−0.01	−2999.97	1732.24	0.13
12	−4000.00	0.00	−0.02	−4000.00	0.07	0.05
13	−3000.00	−1732.05	−0.01	−2999.99	−1731.92	−0.01
14	−2000.00	−3464.11	−0.02	−2000.10	−3464.02	0.02
15	0.00	−3464.11	−0.01	−0.08	−3464.05	0.14
16	2000.00	−3464.11	−0.02	1999.96	−3464.17	−0.19
17	3000.00	−1732.05	−0.01	3000.01	−1731.94	−0.05
18	4000.00	0.00	−0.02	4000.02	0.06	−0.08
19	3000.00	1732.05	−0.01	3000.05	1732.15	−0.09
rms			0.02			0.11

(b) Measured from photogrammetry with gravity load and comparison with analytical predictions

Node	Measured node positions			Difference (Measured − Predicted)		
	X, mm	Y, mm	Z, mm	X, mm	Y, mm	Z, mm
1	−0.05	0.24	0.08	−0.05	0.18	−0.10
2	1000.14	1732.22	0.08	0.12	0.13	0.00
3	−1000.26	1732.17	−0.01	−0.28	0.03	0.06
4	−2000.07	0.12	0.17	−0.09	0.00	0.17
5	−1000.17	−1731.93	0.25	−0.14	0.12	0.08
6	1000.08	−1732.12	0.06	0.04	−0.10	−0.02
7	2000.06	0.21	0.06	0.05	0.13	0.05
8	1999.97	3464.05	−0.15	0.02	−0.15	−0.18
9	0.10	3464.07	−0.19	0.08	−0.01	−0.06
10	−1999.98	3464.03	−0.27	−0.07	−0.21	−0.03
11	−3000.07	1732.03	0.19	−0.10	−0.21	0.05
12	−4000.19	−0.06	0.05	−0.19	−0.13	0.00
13	−3000.02	−1731.75	0.02	−0.03	0.16	0.03
14	−1999.92	−3463.76	−0.11	0.17	0.27	−0.13
15	0.00	−3464.08	0.05	0.08	−0.02	−0.09
16	1999.85	−3463.99	−0.26	−0.12	0.18	−0.08
17	3000.16	−1731.92	0.04	0.15	0.03	0.09
18	4000.23	−0.25	−0.02	0.21	−0.31	0.06
19	3000.20	1732.08	−0.01	0.15	−0.07	0.08
rms			0.14	0.13	0.15	0.09

Table 2. Truss Node Positions Measured in Repeatability Tests

[Referenced to predicted locations]

Node	Predicted node locations (member error and gravity)			Measured node positions (test A)		
	X, mm	Y, mm	Z, mm	X, mm	Y, mm	Z, mm
1	−0.01	0.05	0.18	−0.14	0.08	0.41
2	1000.01	1732.10	0.08	1000.07	1732.21	0.12
3	−999.98	1732.14	−0.07	−1000.25	1732.15	0.03
4	−1999.98	0.11	0.00	−2000.03	−0.02	0.04
5	−1000.03	−1732.06	0.16	−1000.24	−1732.02	0.14
6	1000.04	−1732.01	0.08	1000.14	−1732.25	0.08
7	2000.01	0.08	0.01	2000.03	0.24	0.14
8	1999.94	3464.21	0.03	1999.80	3464.02	−0.09
9	0.01	3464.08	−0.15	0.08	3463.98	−0.27
10	−1999.92	3464.23	−0.27	−1999.85	3463.90	−0.10
11	−2999.98	1732.23	0.14	−2999.94	1732.05	0.07
12	−4000.00	0.05	0.08	−4000.05	0.01	−0.26
13	−2999.98	−1731.93	0.00	−2999.92	−1731.88	0.05
14	−2000.07	−3464.04	0.00	−1999.91	−3464.02	−0.04
15	−0.05	−3464.05	0.15	−0.05	−3464.23	−0.01
16	2000.00	−3464.20	−0.20	2000.00	−3464.18	−0.27
17	3000.01	−1731.94	−0.04	3000.11	−1731.88	−0.04
18	4000.03	0.07	−0.08	4000.27	−0.18	−0.29
19	3000.05	1732.15	−0.09	2999.89	1732.02	0.28
rms			0.12			0.18

Node	Measured node positions (test B)			Difference (Test B − Test A)		
	X, mm	Y, mm	Z, mm	X, mm	Y, mm	Z, mm
1	−0.11	0.02	0.44	0.04	−0.06	0.03
2	1000.11	1732.26	0.15	0.04	0.05	0.03
3	−1000.22	1732.19	0.06	0.03	0.04	0.03
4	−2000.03	−0.06	0.12	0.00	−0.04	0.08
5	−1000.22	−1732.09	0.21	0.02	−0.07	0.07
6	1000.12	−1732.25	0.07	−0.02	0.00	0.00
7	2000.02	0.27	0.11	−0.01	0.03	−0.03
8	1999.83	3464.00	−0.06	0.03	−0.02	0.03
9	0.12	3464.05	−0.28	0.04	0.07	−0.01
10	−1999.83	3463.90	−0.13	0.03	0.00	−0.04
11	−3000.05	1732.11	0.08	−0.11	0.06	0.00
12	−4000.15	−0.01	−0.33	−0.10	−0.02	−0.08
13	−2999.93	−1731.96	0.03	−0.01	−0.07	−0.02
14	−1999.95	−3464.11	−0.08	−0.03	−0.09	−0.05
15	−0.05	−3464.14	0.04	0.00	0.09	0.05
16	1999.97	−3464.17	−0.29	−0.03	0.01	−0.02
17	3000.13	−1731.93	−0.05	0.02	−0.05	−0.01
18	4000.28	−0.17	−0.33	0.00	0.01	−0.04
19	2999.95	1732.08	0.25	0.06	0.07	−0.03
rms			0.20	0.04	0.05	0.04

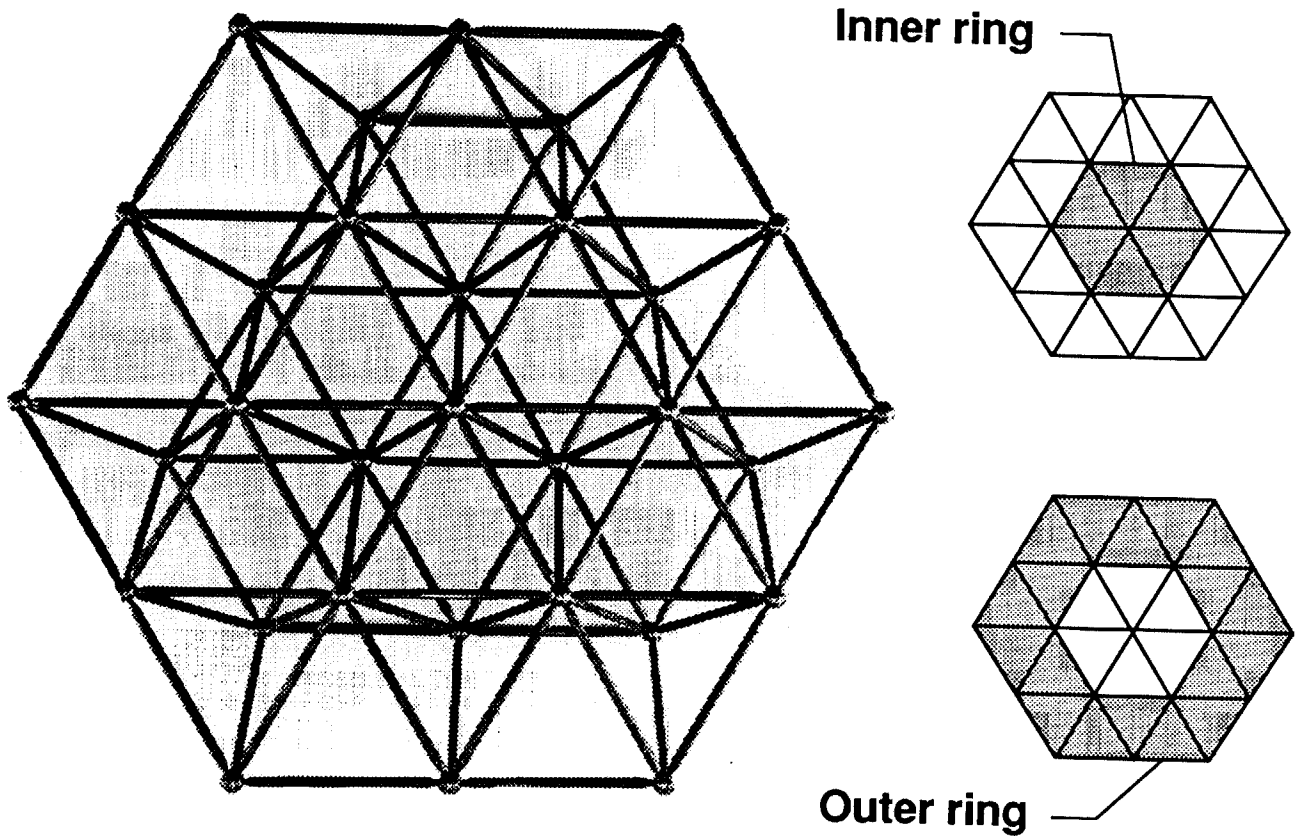

Figure 1. Planform view of planar tetrahedral truss.

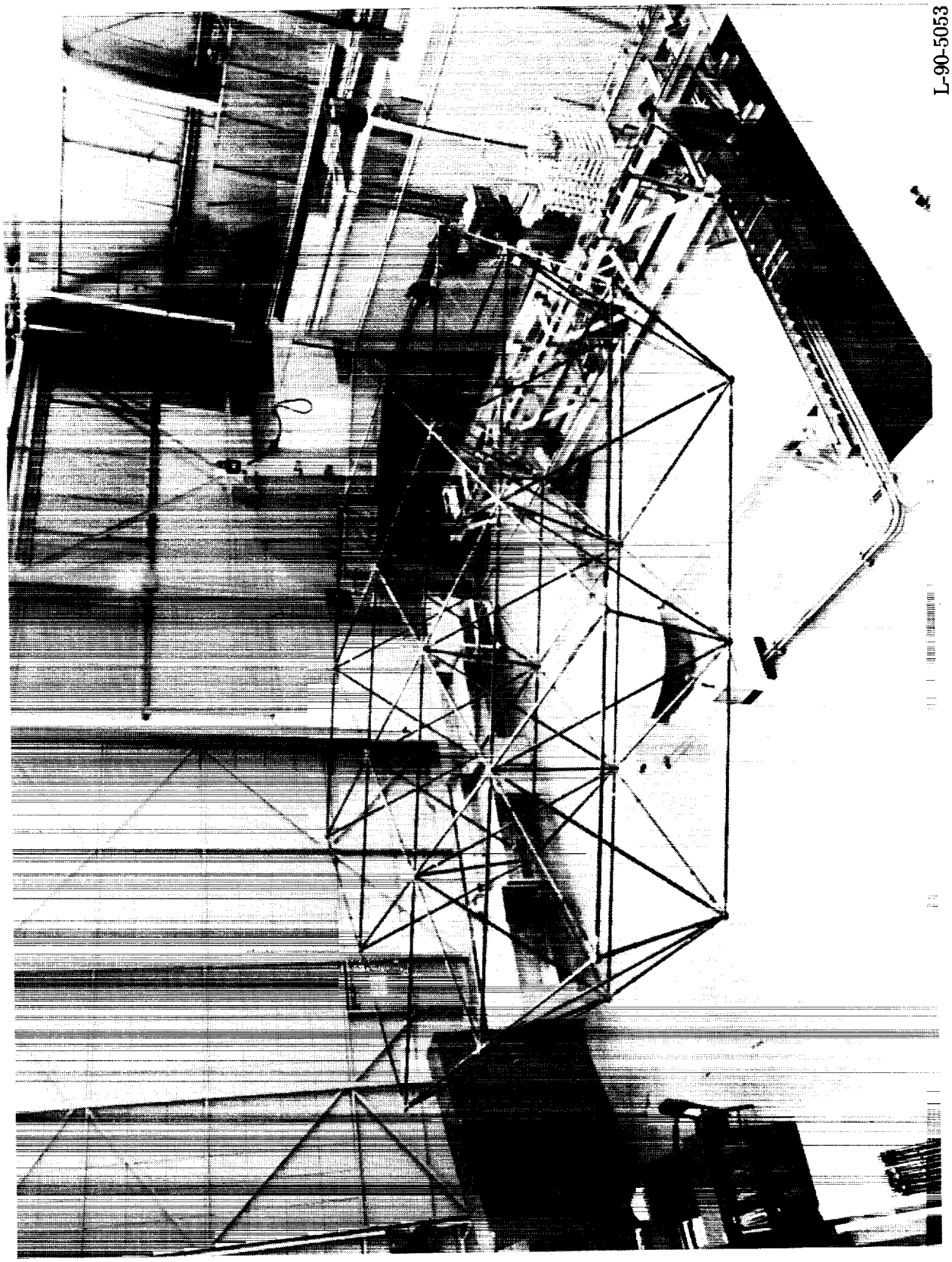

L-90-5053

Figure 2. Assembled tetrahedral truss test hardware.

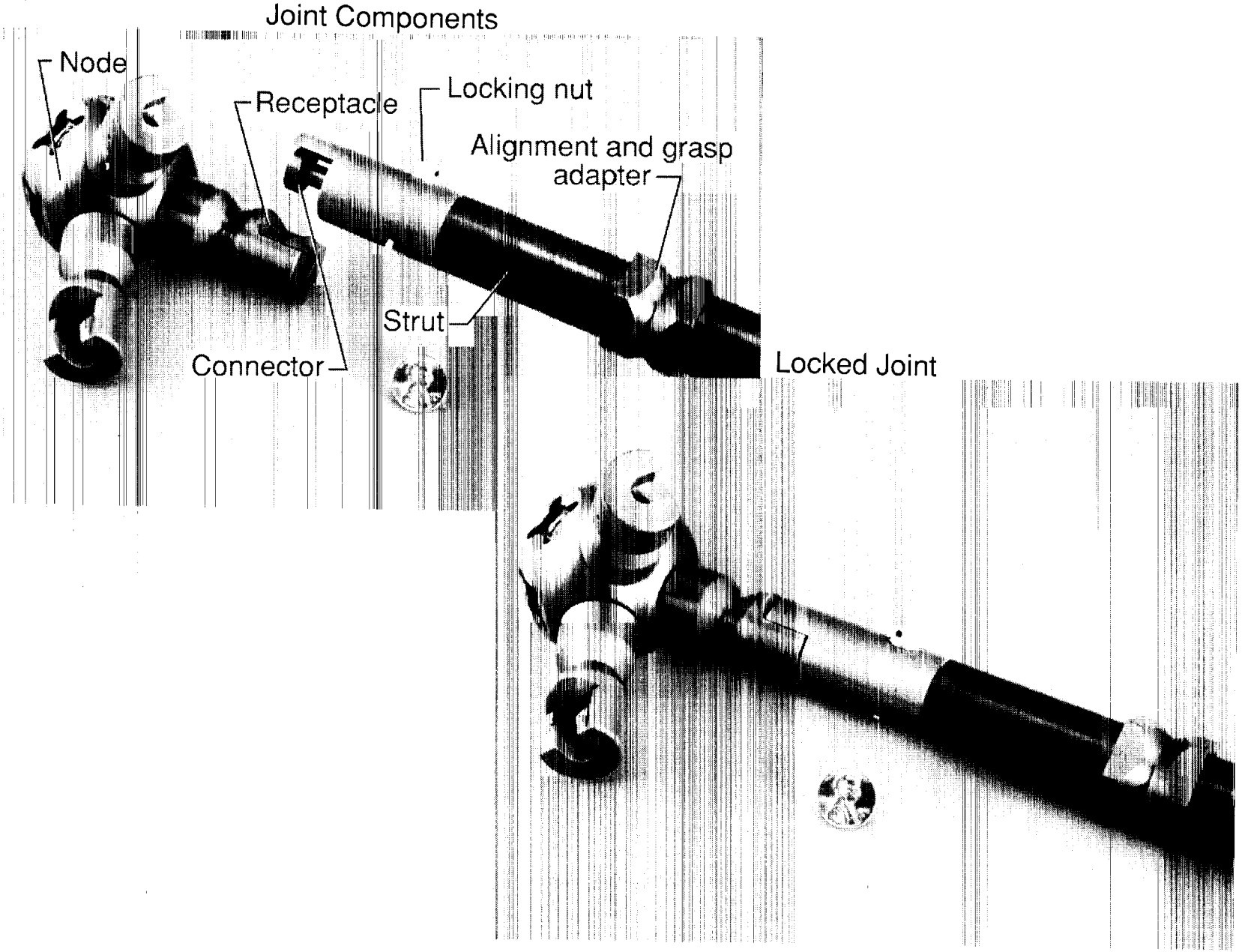

Figure 3. Mechanically preloaded joint.

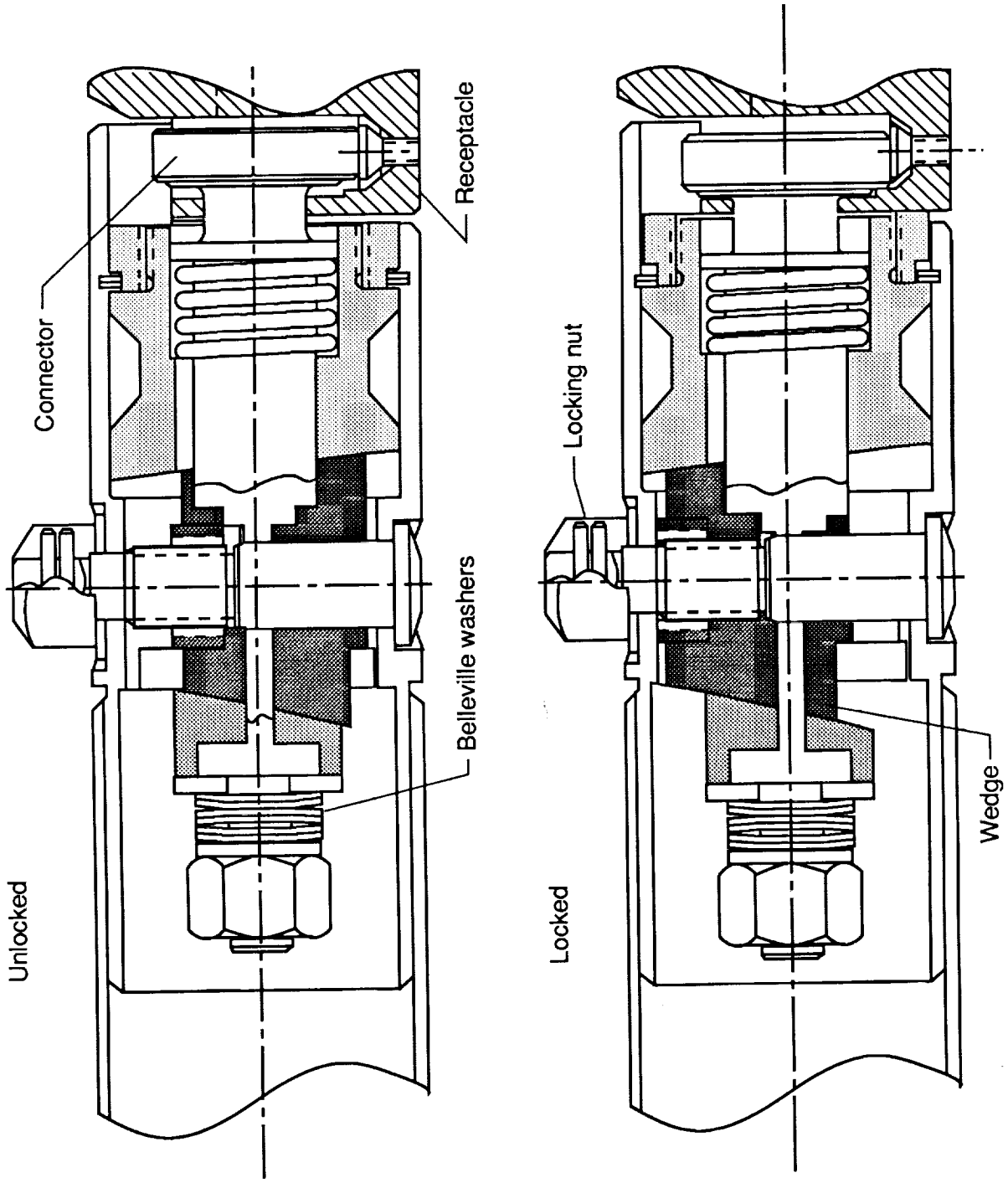

Figure 4. Joint internal mechanism.

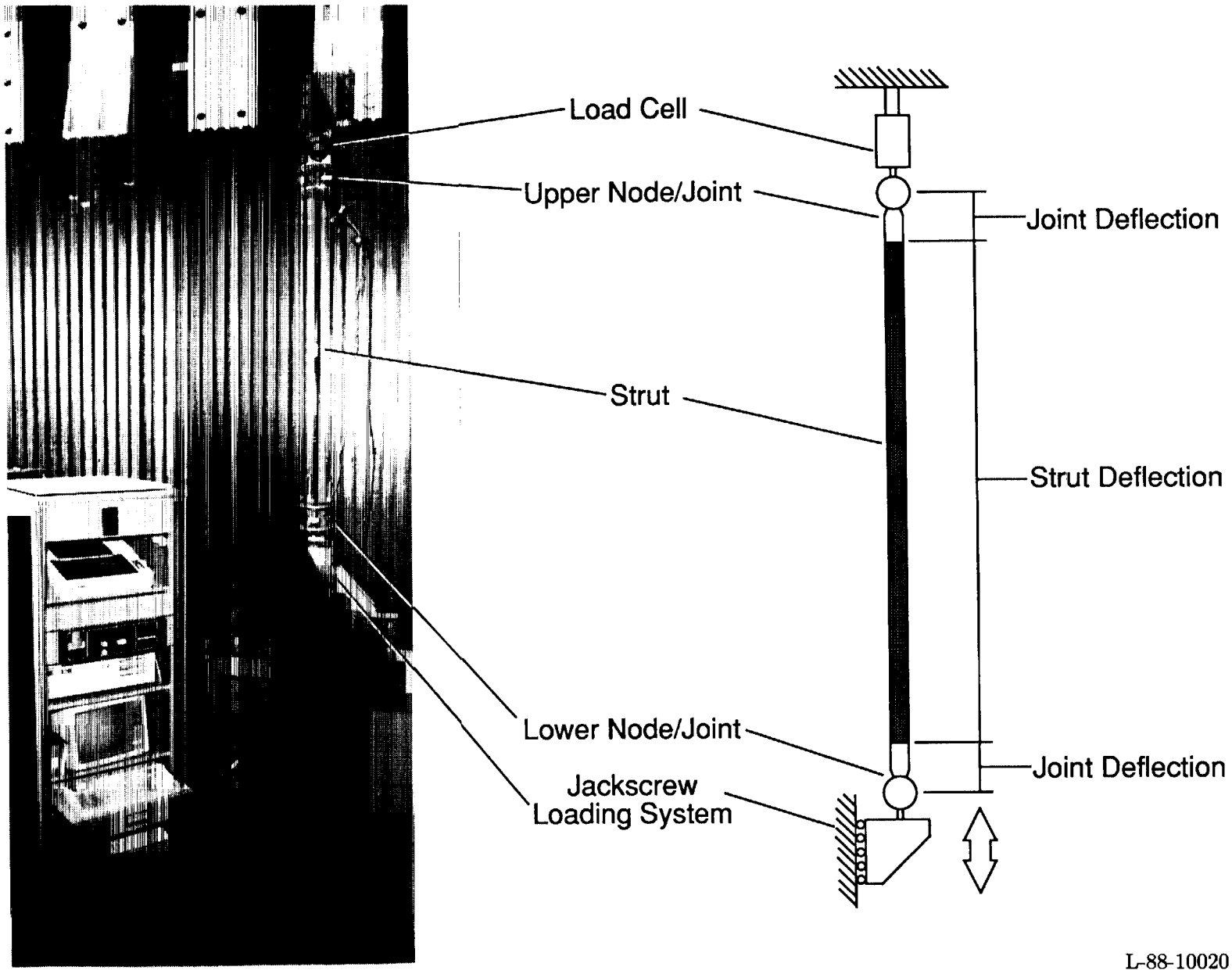

Figure 5. Experimental test setup used to evaluate strut stiffness.

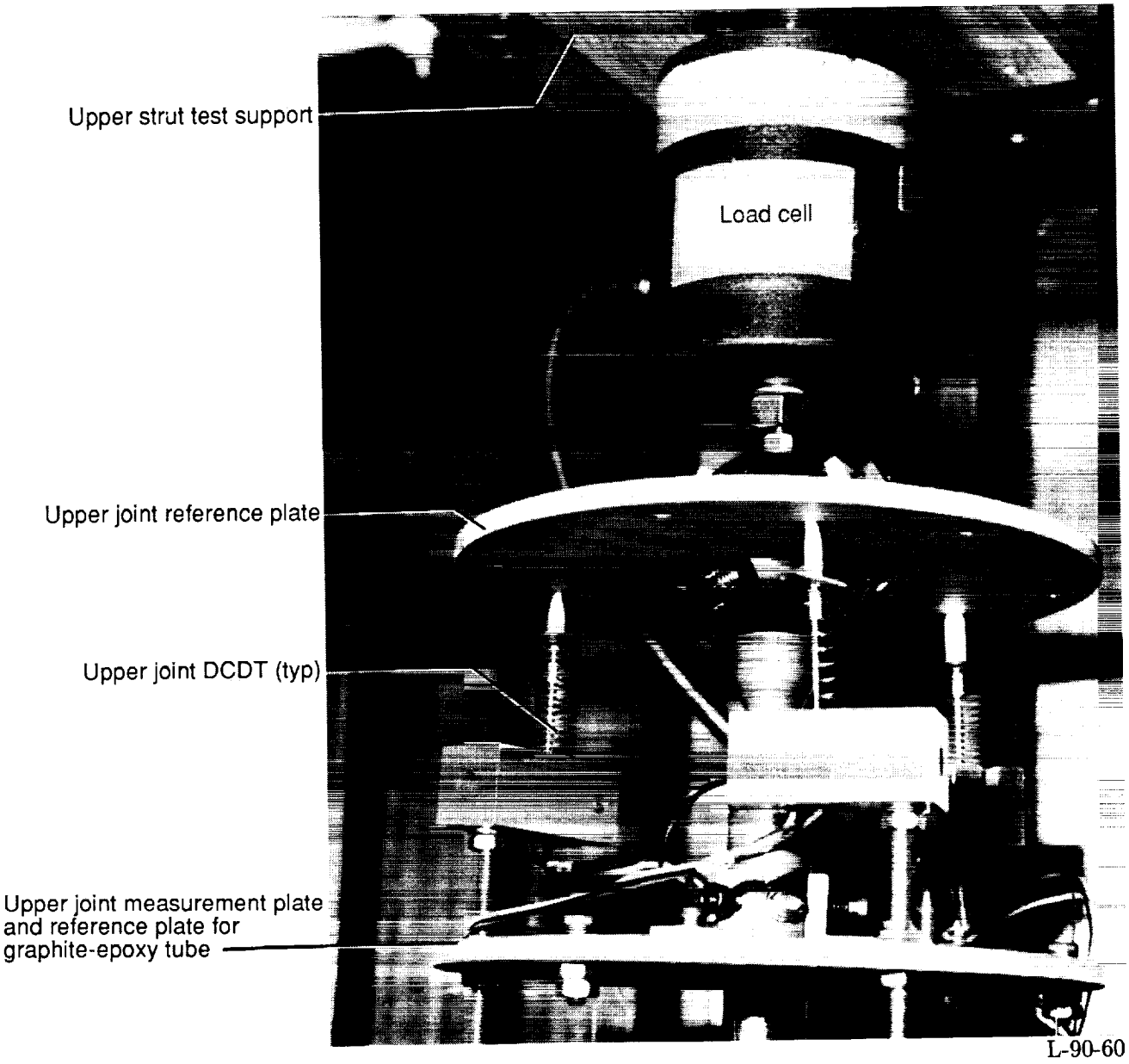

(a) Load cell and displacement DCDT's for upper joint.

Figure 6. Instrumentation setup for strut stiffness evaluation.

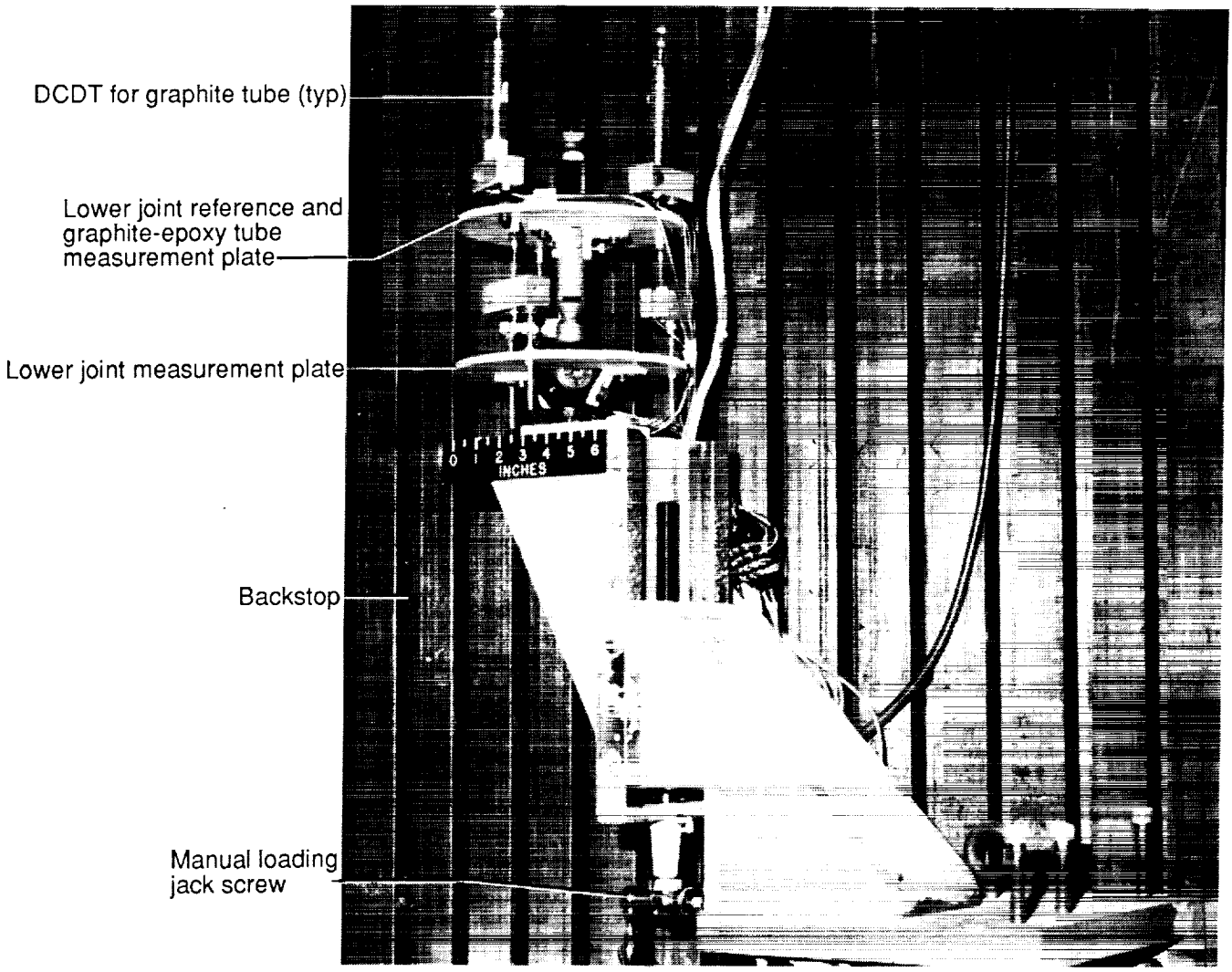

L-90-61

(b) Strut jackscrew loading system and displacement DCDT's for lower joint and graphite-epoxy tube.

Figure 6. Concluded.

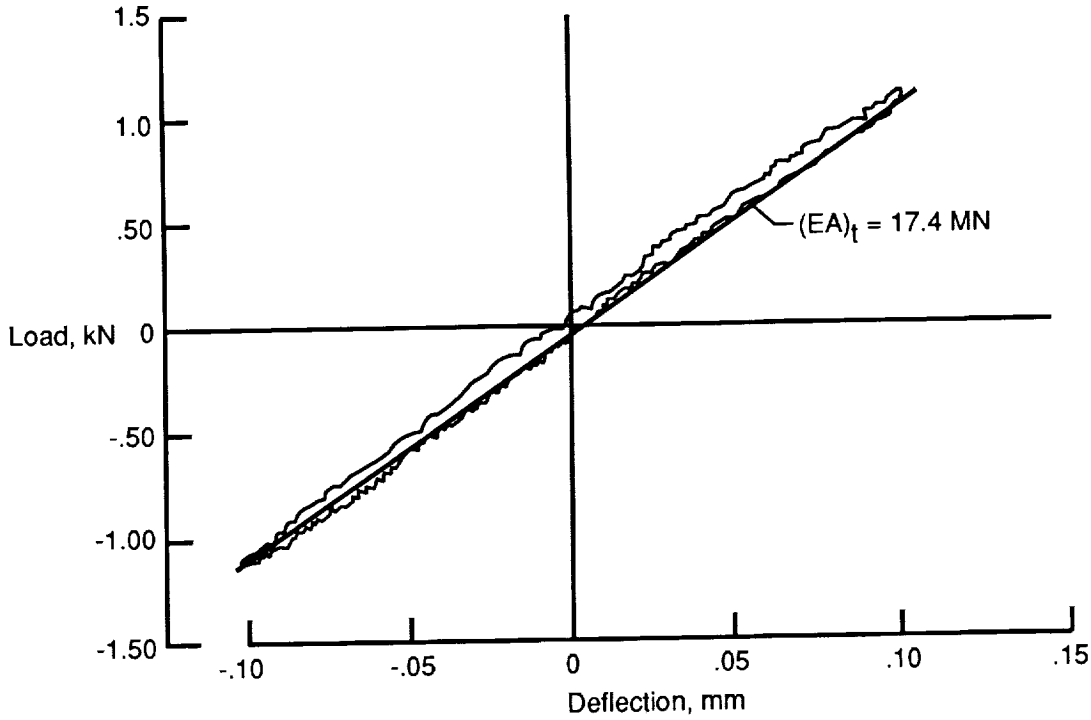

Figure 7. Load-displacement data from tests on graphite-epoxy strut tube.

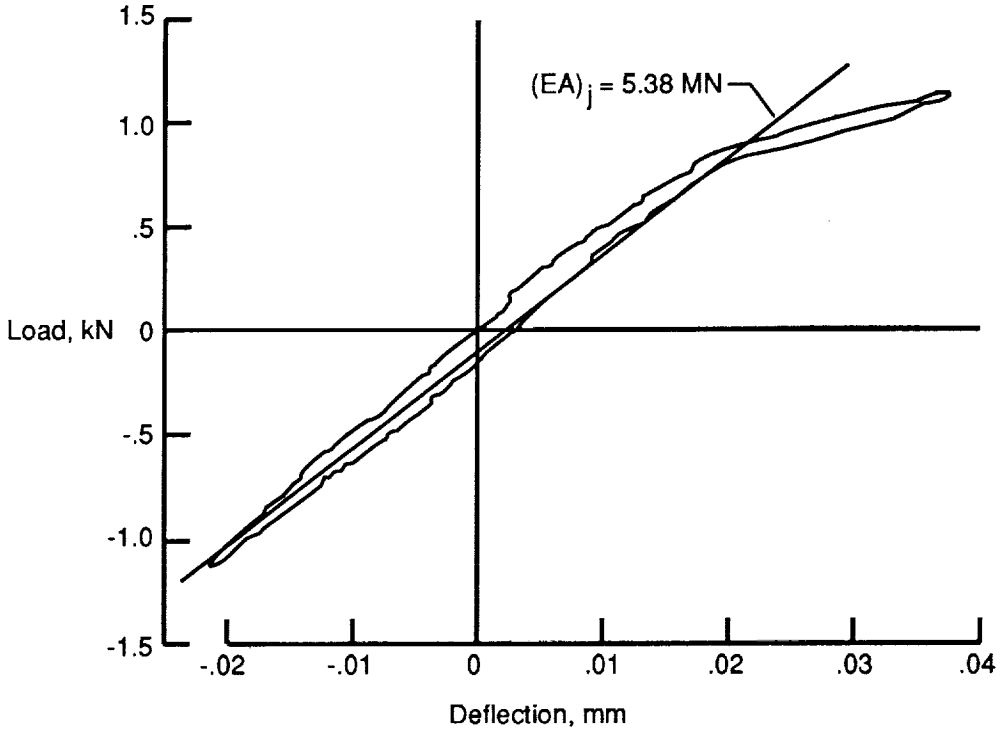

(a) Test joint with nominal tensile preload.

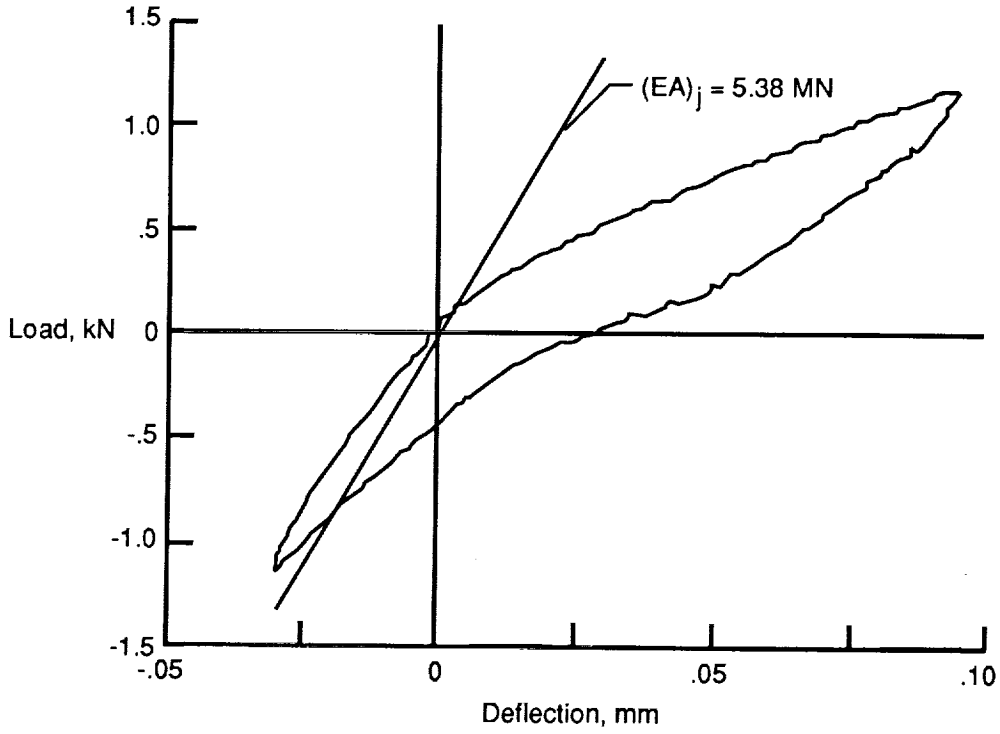

(b) Test joint with low tensile preload.

Figure 8. Load-displacement data from tests on truss joints.

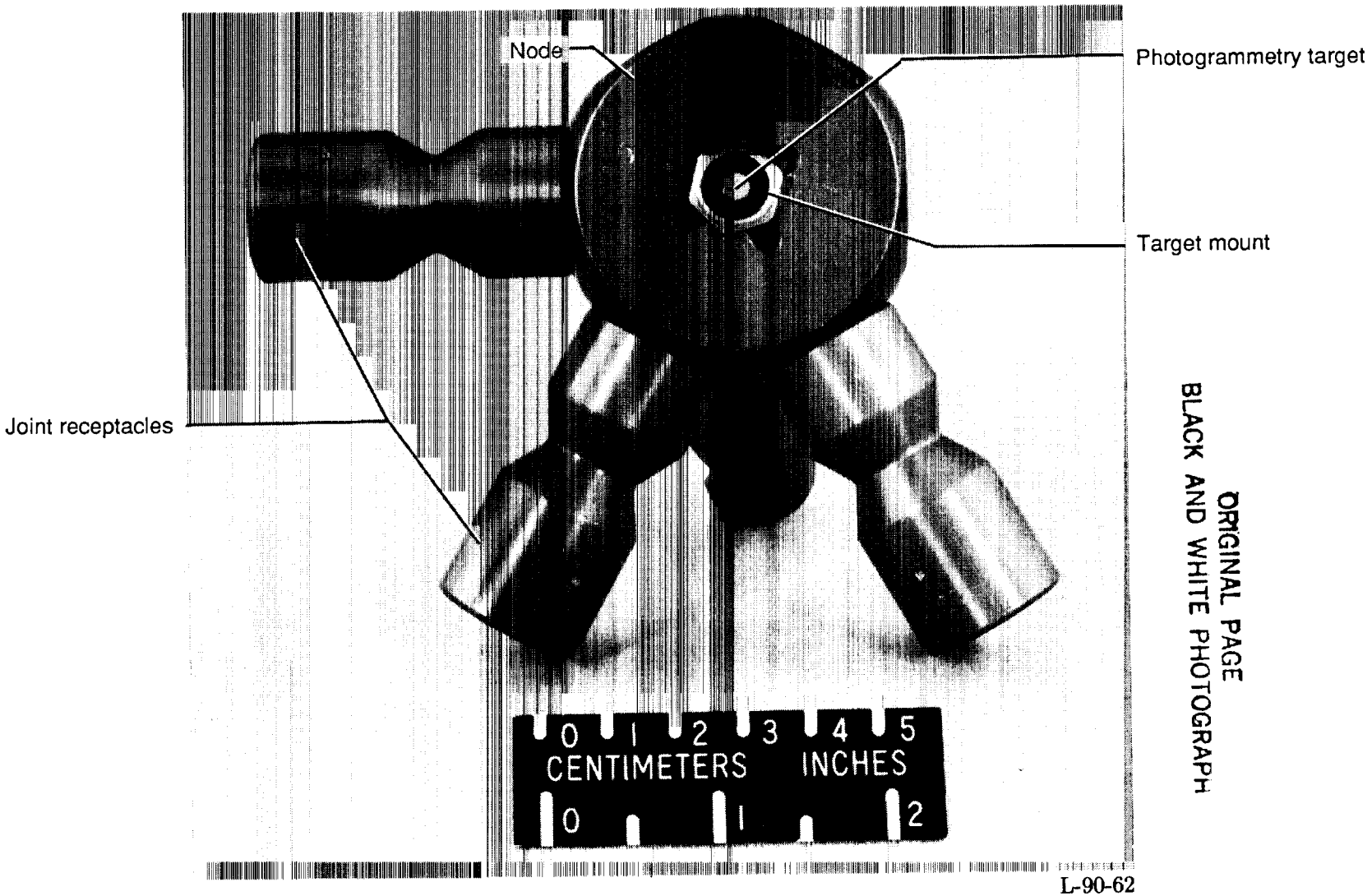

ORIGINAL PAGE
BLACK AND WHITE PHOTOGRAPH

Figure 9. Truss node with attached photogrammetry target mount.

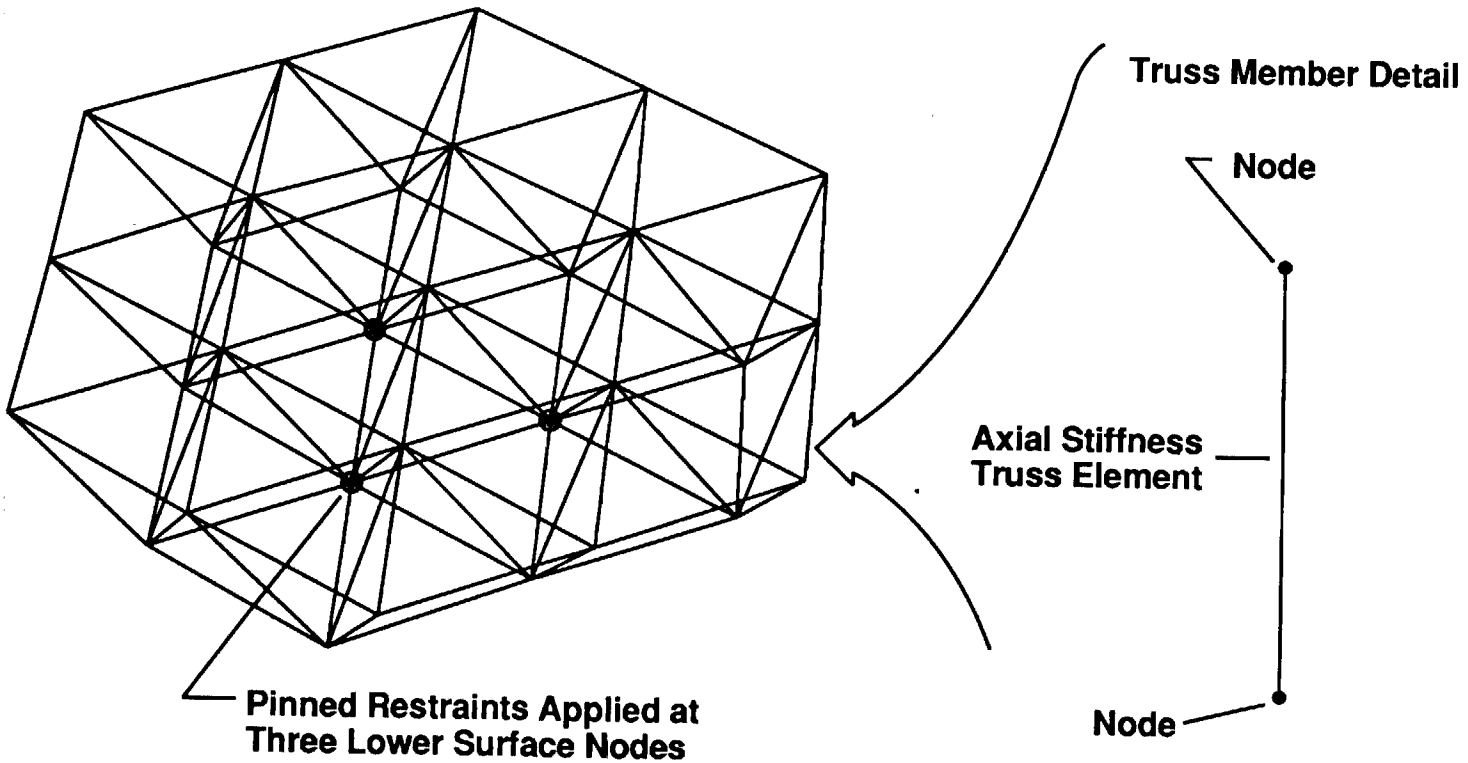

Figure 10. Finite element model of tetrahedral truss structure.

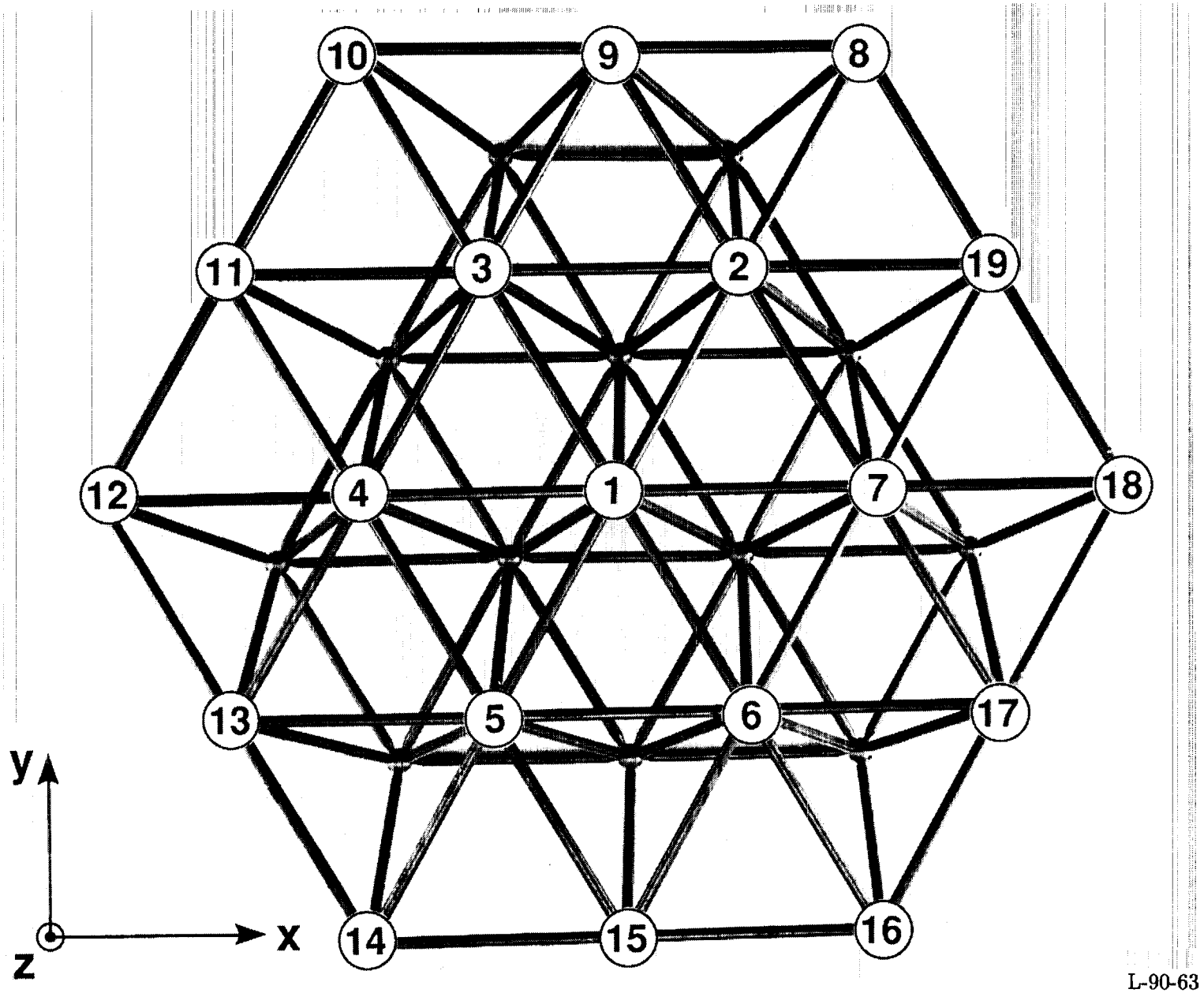

Figure 11. Numbering sequence of truss upper surface nodes for both analytical and experimental evaluation.

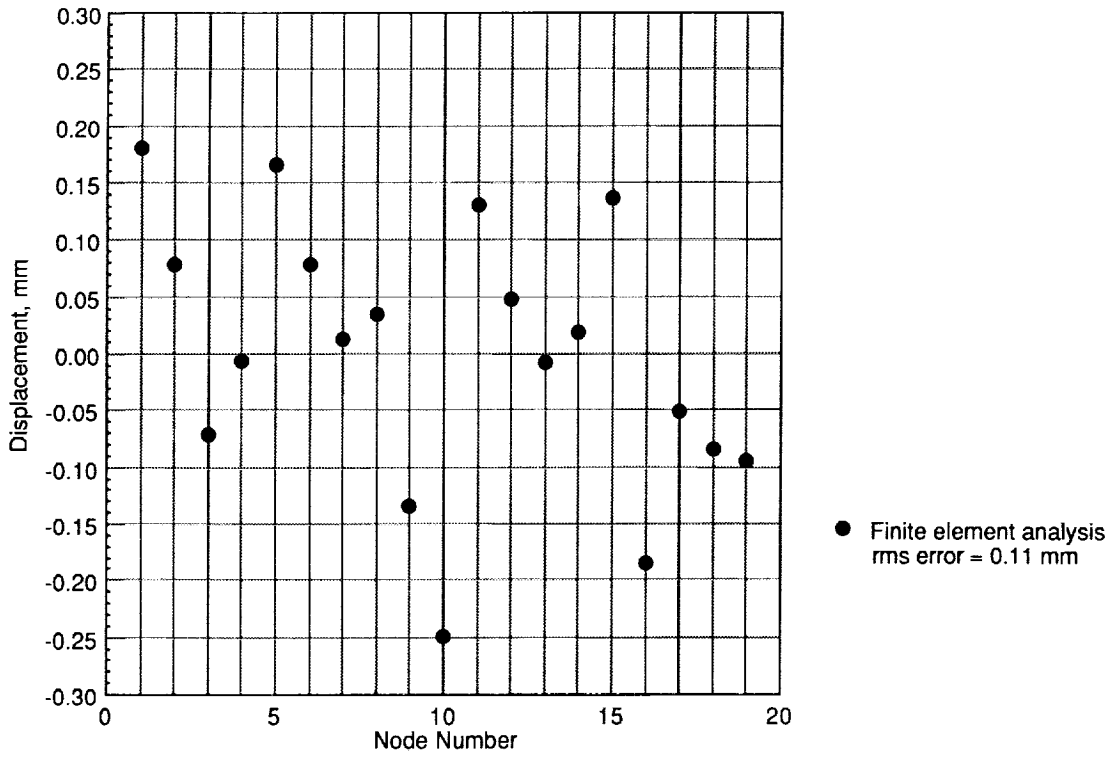

(a) Normal displacement from best-fit plane as function of node number.

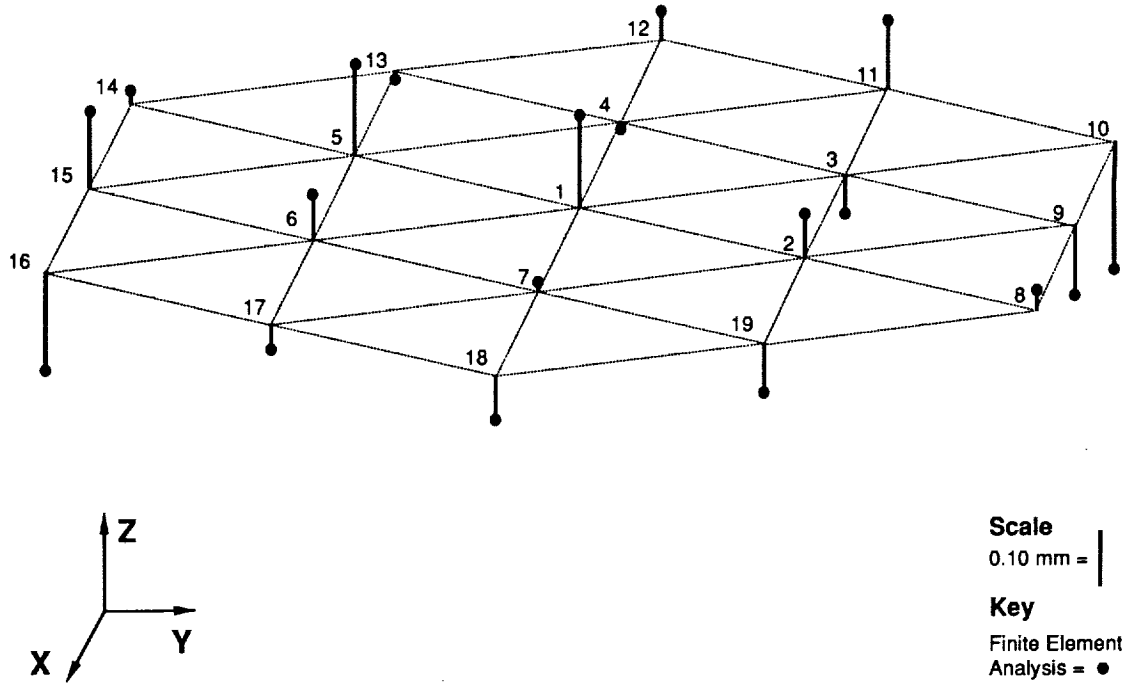

(b) Axonometric projection illustrating normal displacement of nodes.

Figure 12. Analytically predicted normal displacement of truss upper surface nodes.

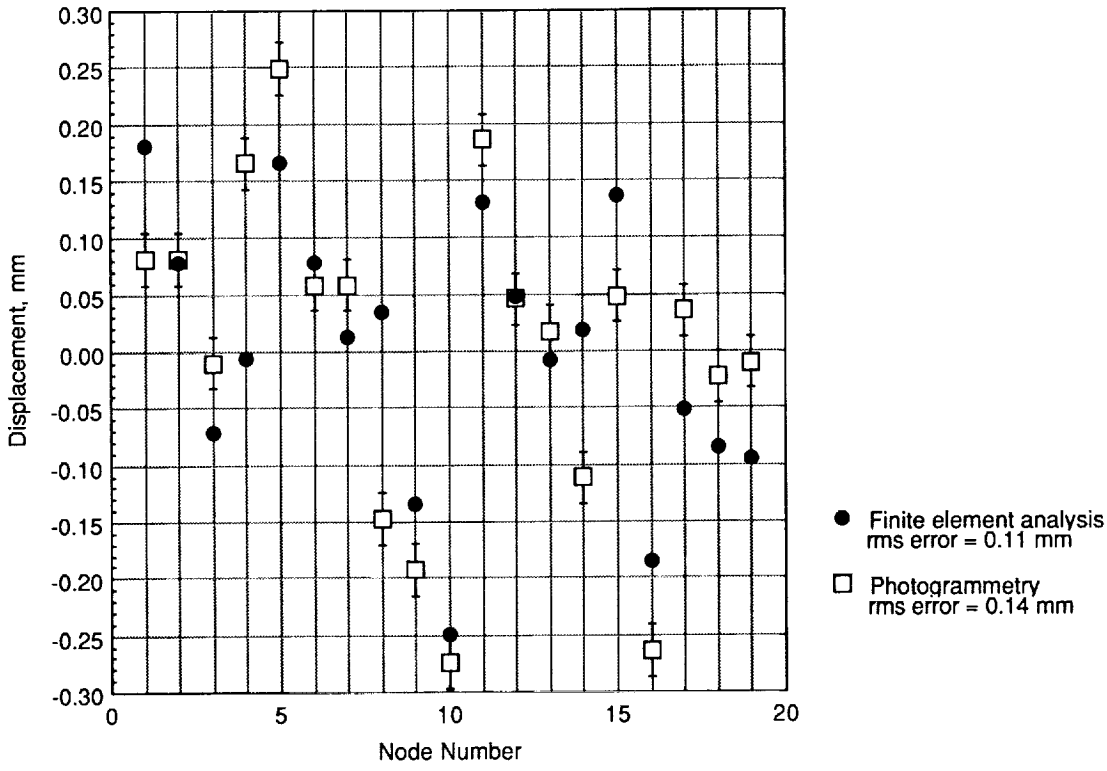

(a) Normal displacement from best-fit plane as function of node number.

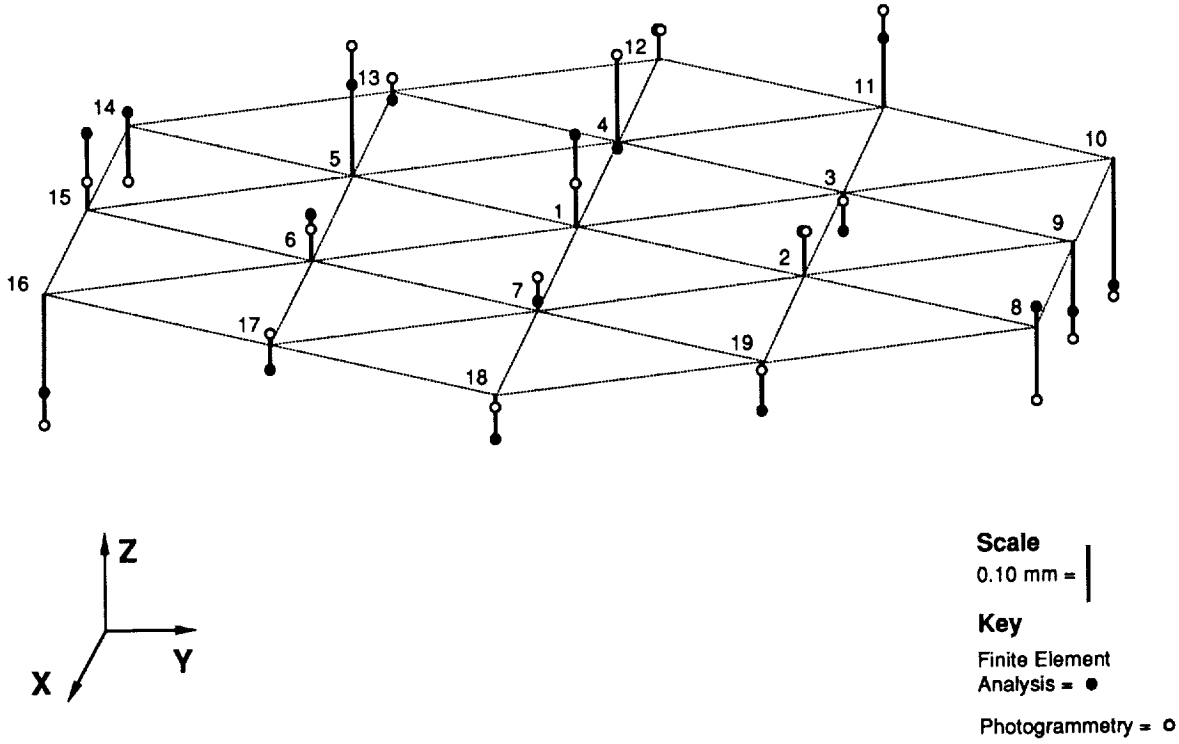

(b) Axonometric projection illustrating normal displacement of nodes.

Figure 13. Test measurement and analysis prediction of normal displacement of truss upper surface nodes.

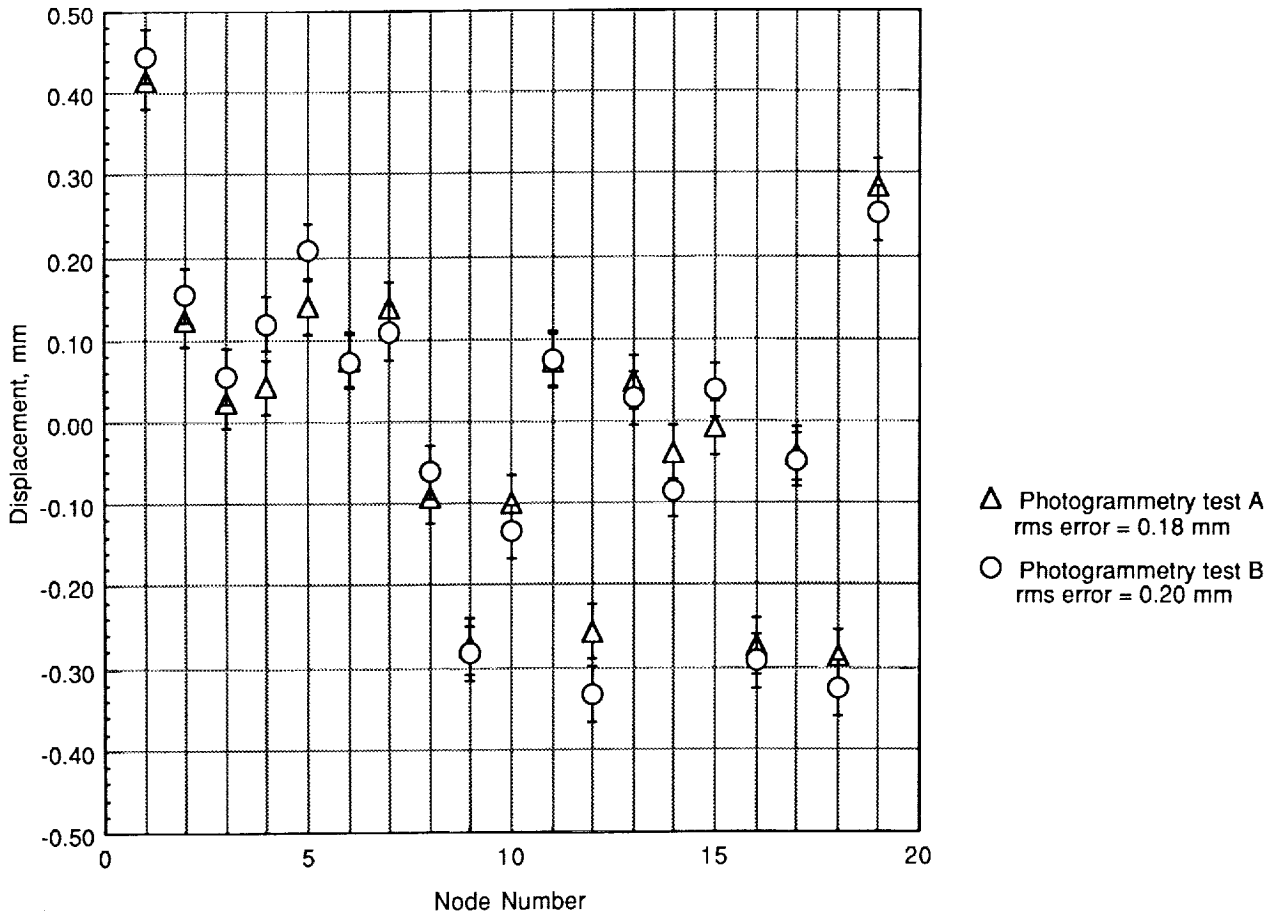

Figure 14. Photogrammetry measurement of normal displacements of truss nodes from best-fit plane to evaluate repeatability of node position for assembly tests.

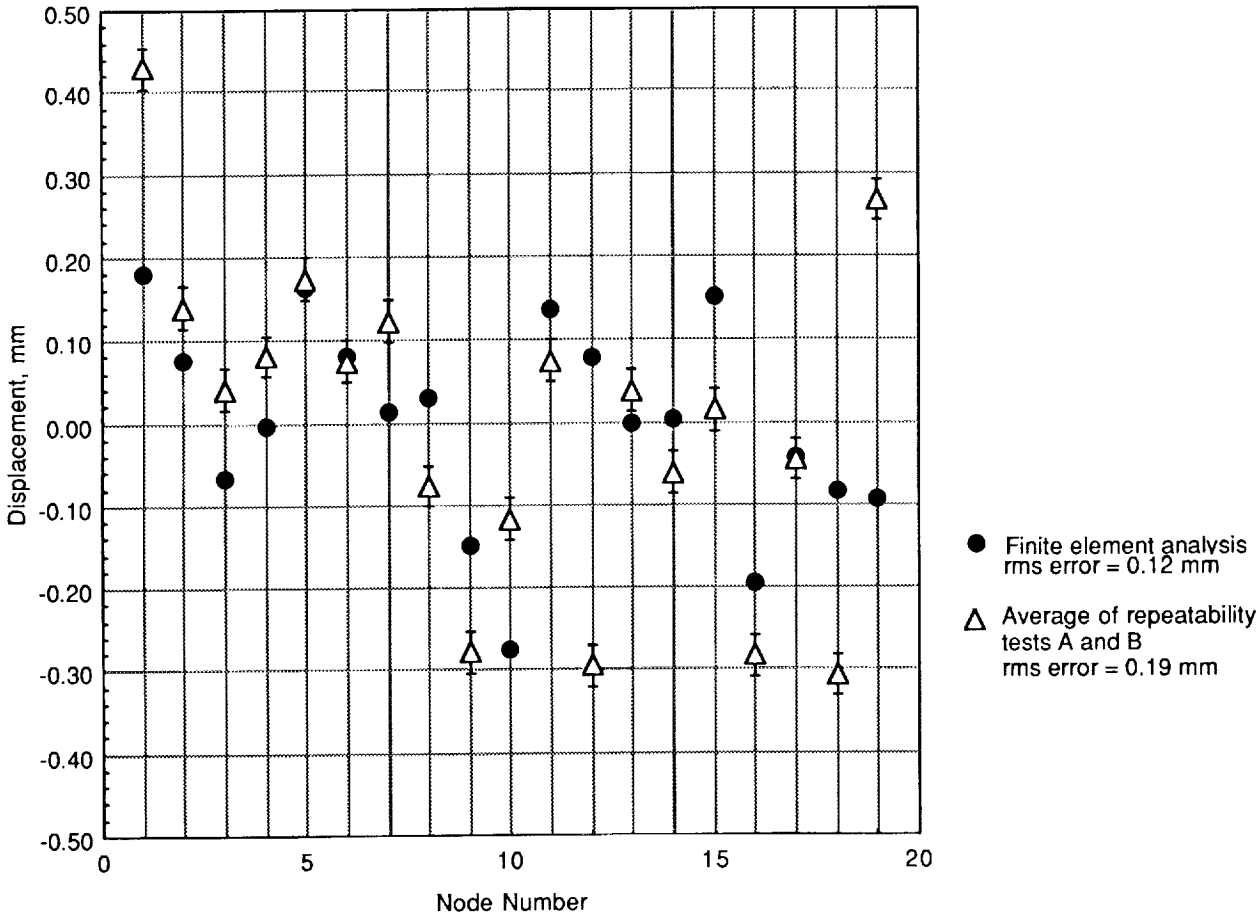

Figure 15. Test measurement and analysis prediction of normal displacement of truss nodes from best-fit plane for assembly repeatability tests.

NASA
National Aeronautics and Space Administration

Report Documentation Page

1. Report No.	2. Government Accession No.	3. Recipient's Catalog No.
NASA TM-4231		

4. Title and Subtitle	5. Report Date
Analytical and Photogrammetric Characterization of a Planar Tetrahedral Truss	December 1990
	6. Performing Organization Code
7. Author(s)	8. Performing Organization Report No.
K. Chauncey Wu, Richard R. Adams, and Marvin D. Rhodes	L-16758
9. Performing Organization Name and Address	10. Work Unit No.
NASA Langley Research Center Hampton, VA 23665-5225	506-43-41-02
	11. Contract or Grant No.
12. Sponsoring Agency Name and Address	13. Type of Report and Period Covered
National Aeronautics and Space Administration Washington, DC 20546-0001	Technical Memorandum
	14. Sponsoring Agency Code

15. Supplementary Notes

16. Abstract

Proposed large, space-based telescopes and antennas will require a reflective surface free from distortions which would significantly degrade the reflector accuracy. It is desirable to be able to analytically predict and experimentally verify the attachment point locations of these structures prior to use in space-flight applications. An investigation was conducted to evaluate the upper surface planarity of a tetrahedral truss structure with both finite element analyses and close-range photogrammetric methods. Reasonable correlation between the predicted and measured upper surface node positions was observed, with a measured root-mean-square (rms) surface error of 0.14 mm. In addition, the repeatability of the truss was within the measurement precision of the photogrammetry technique.

17. Key Words (Suggested by Authors(s))	18. Distribution Statement
Large space structures Precision trusses Photogrammetry Antenna surface accuracy	Unclassified—Unlimited Subject Category 18

19. Security Classif. (of this report)	20. Security Classif. (of this page)	21. No. of Pages	22. Price
Unclassified	Unclassified	28	A03

NASA FORM 1626 OCT 86

NASA-Langley, 1990

For sale by the National Technical Information Service, Springfield, Virginia 22161-2171